Chem Soc Rev

REVIEW ARTICLE

View Article Online
View Journal

Cite this: DOI: 10.1039/d5cs01279a

Nano-structuring hydrogen-bonded organic frameworks: strategies, composites, and functional applications

Qiang Zhu[ab] and Antonio Fernandez *[ac]

Hydrogen-bonded organic frameworks are a rising class of porous materials that are now recognized for their high surface areas, mild synthesis, solution processability, and biocompatibility, making them attractive for a wide range of applications. However, their bulk forms often suffer from limitations such as poor electrical conductivity and insufficient structural stability, which can hinder practical implementation. To transcend the limitations of their bulk counterparts, a powerful strategy is their transformation into pristine nanostructures or nanocomposites, which enhances properties such as conductivity, stability, and porosity. These HOF nanomaterials leverage the synergistic effects of nanoconfinement and composite matrices, leading to enhanced performance in applications ranging from photocatalysis and energy storage to photothermal therapy. This review aims to provide an overview of recent developments, focusing on the classification, fabrication strategies, and diverse applications of HOF nanomaterials, thereby offering a perspective for future research in this evolving field.

Received 29th January 2026

DOI: 10.1039/d5cs01279a

rsc.li/chem-soc-rev

1. Introduction

Hydrogen-bonded organic frameworks (HOFs) are an emerging class of porous molecular materials assembled *via* non-covalent hydrogen bonding, distinguishing them from covalent organic frameworks (COFs)[1,2] and metal–organic frameworks (MOFs).[3,4] The origin of HOFs can be tracked to 1969, when Duchamp

[a] *Chemistry Department, Loughborough University, Loughborough LE11 3TU, UK*
[b] *State Key Laboratory of Natural Product Chemistry, College of Chemistry and Chemical Engineering, Lanzhou University, Lanzhou, Gansu 730000, China*
[c] *Facultad de Ciencias, Avenida Fuente nueva s/n, Universidad de Granada, Spain. E-mail: antoniofernandez@ugr.es*

Qiang Zhu

Dr Qiang Zhu earned his MS degree in 2018 from Lanzhou University under the supervision of Prof. Wei Wang. He then moved to the University of Liverpool, where he completed his PhD in 2022 under the guidance of Prof. Andrew I. Cooper. Following his doctorate, Dr Zhu undertook postdoctoral research, working successively in the groups of Prof. Cooper (2022–2025) and Dr Fernandez (2025–2026). In 2026, he joined Lanzhou University to establish his independent research group. His research focuses on the precise assembly of functional molecules and organic cages, with an in-depth exploration of their structure–property relationships at the atomic scale.

Antonio Fernandez-Mato

Antonio Fernandez was a Senior Lecturer at Loughborough University (UK), and he is currently a Beatriz Galindo Fellow (since February 2026) at Universidad de Granada (Spain). Throughout his career, he has been working in the field of supramolecular materials, focusing on the synthesis and characterization of molecular machines, materials for nanofabrication and nanolithography, and nanoporous materials for catalytic and sensor applications. Recently, he has also focused on the chemical recycling of different types of waste.

and Marsh reported the crystal structure of trimesic acid, which forms a honeycomb-like network featuring interpenetrating hexagonal channels—a foundational prototype of a HOF.[5] In the 1990s, Wuest and colleagues pioneered the field by introducing the 'molecular tectonics' strategy.[6,7] They synthesized tetrahedral building blocks that self-assembled into three-dimensional (3D) diamondoid networks with guest-accessible voids, conceptualizing the design of hydrogen-bonded networks. However, the inherent weakness and flexibility of hydrogen bonds often resulted in structure collapse upon guest removal, hindering HOF development and causing the field to lag behind MOFs and COFs for years. A breakthrough came two decades later when Chen and co-workers demonstrated the first HOF with permanent porosity *via* gas sorption and formally coined the term 'hydrogen-bonded organic frameworks'.[8] This milestone ignited renewed interest in HOFs, and the field has since evolved rapidly, increasingly leveraging computation-assisted design and automation to accelerate the discovery of stable, functional materials.[9–11] In 2012, Mastalerz *et al.* achieved a breakthrough by increasing the Brunauer–Emmett–Teller (BET) surface area of HOFs to 2796 $m^2\ g^{-1}$ using a triptycene-based building block (TTBI).[12] In 2015, Chen *et al.* reported a flexible HOF exhibiting high performance for CO_2 capture.[13] In 2017, guided by crystal structure prediction (CSP), Cooper, Day, and coworkers discovered three new polymorphs of TTBI, including one with a record-high surface area of 3425 $m^2\ g^{-1}$.[11] Later, Cao and Liu developed a widely used robust HOF, termed PFC-1, based on a pyrene core with an extended π-conjugated system.[14] In 2019, Falcaro and Doonan *et al.* pioneered the use of HOFs for enzyme stabilization.[15] Most recently, Bu, Chen, Li, and their teams have showcased the potential of flexible HOFs for gas separation, achieving an exceptional SO_2/CO_2 selectivity of 7331 and a high SO_2 storage density of 3.27 g cm^{-3} under ambient conditions.[16] Owing to their desirable properties, such as large BET surface areas, mild synthetic conditions, good solution processability, and excellent biocompatibility,[17] HOFs have demonstrated great potential for practical applications, including gas separation, sensing, catalysis, and energy storage.[18–20]

Nanomaterials, broadly defined as functional materials with at least one structural dimension confined to the nanoscale (typically <100 nm), often exhibit properties dramatically distinct from their bulk counterparts.[21] A key advantage lies in their ability to function as composite matrices, integrating the merits of different components to achieve enhanced synergistic functionalities. Among various substrates, HOFs have emerged as particularly attractive candidates due to their excellent solution processability and high functional tunability.

Transforming bulk HOFs into nanostructures and nanocomposites represents a promising strategy for optimizing their functional properties, as evidenced by several key enhancements. For instance, converting bulk HOFs into nanosheets

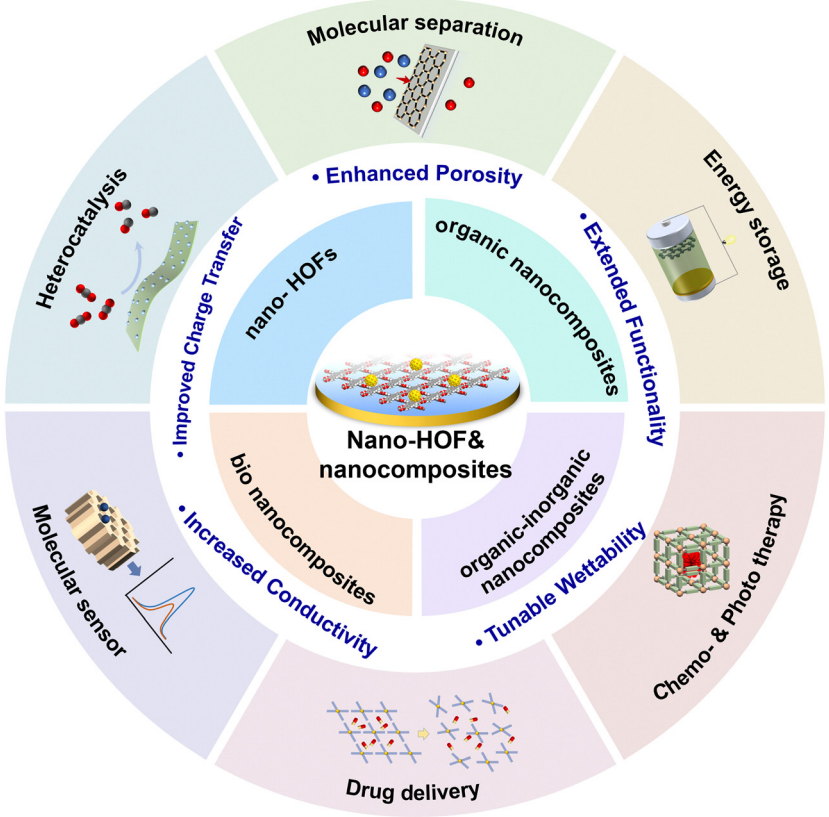

Fig. 1 Summary of categories and applications for nano-HOFs and HOF nanocomposites.

or thin films increases their accessible pore surface area, thereby improving substrate accessibility. Additionally, integrating HOFs with conductive materials such as graphene oxide combines their efficient mass transfer properties with high electrical conductivity, making these composites attractive for electronic device applications. Combining HOFs with other framework materials, such as COFs, can also create heterojunctions that facilitate efficient charge separation, thereby boosting catalytic performance. This strategy also enables the tailoring of surface functionality. By coating substrates with HOFs, surface wettability can be precisely engineered, thereby optimizing reactant affinity, enhancing interfacial mass transport, and improving catalytic efficiency. Finally, employing HOFs as protective shells to encapsulate enzymes can not only stabilize them under harsh conditions but also introduces non-native functions through conformational modulation. These enhancements are expected to expand the materials' performance across a wide range of applications, including heterogeneous catalysis, energy storage, and photothermal therapy, among others (Fig. 1).

Despite a series of recent reviews on HOFs,[22–27] a comprehensive summary of the current investigations in the field of HOF-based nanomaterials remains notably absent.[28] Given this gap, this review aims to provide an overview of the recent developments in HOF-based nanomaterials. We will focus on their fabrication strategies, classification, and diverse applications, offering a promising perspective for future research in this field. To ensure clarity, this review categorizes the materials discussed into two distinct classes:

Pristine nano-HOFs

Materials that retain the intrinsic crystalline HOF structure but are fabricated showing effects. This includes nanosheets (NSs), nanoparticles (NPs), and nanorods (NRs).

HOF nanocomposites

Hybrid materials where HOFs serve as a host matrix or template for incorporating functional nanomaterials (*e.g.*, NPs, quantum dots). Here, the framework structure remains intact, but the functionality is enhanced by the guest species.

2. Nano-structuring strategies

Nano-structuring strategies for HOFs and their nanocomposites fall into three categories based on the fabrication sequence: (i) *in situ* synthesis and assembly, (ii) *in situ* assembly, and (iii) post-conversion (Fig. 2).

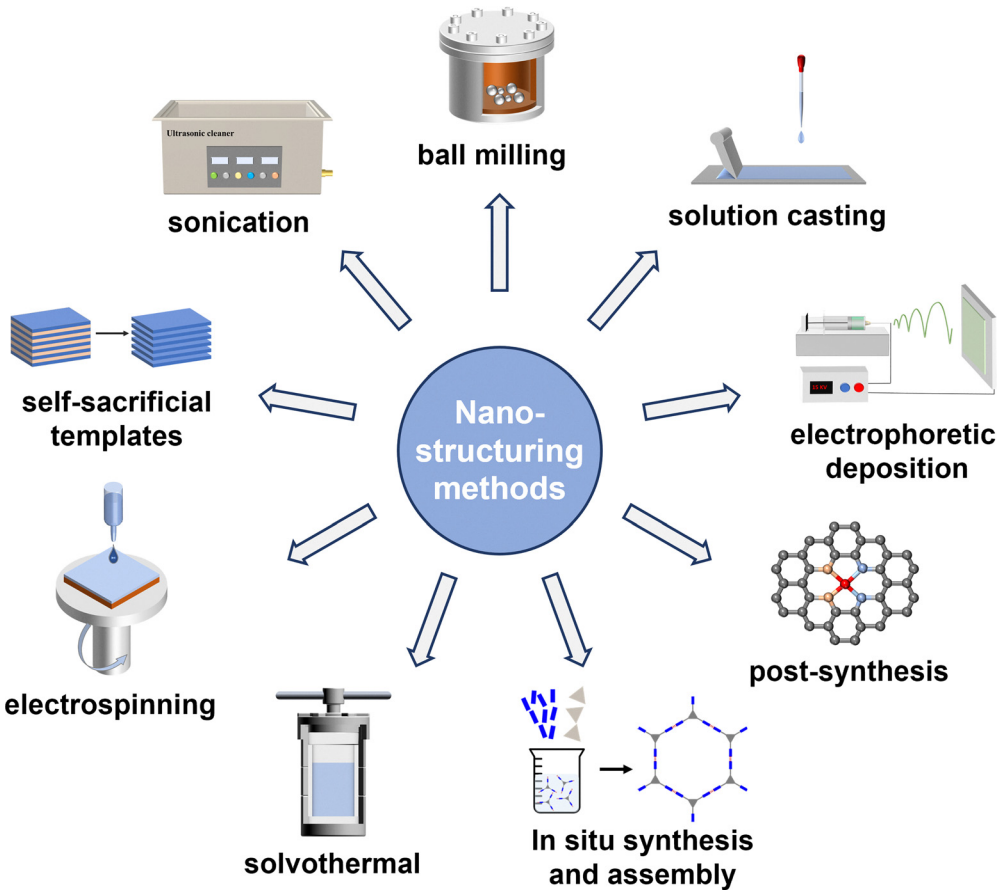

Fig. 2 Most common methods used in the fabrication of HOF nanomaterials.

2.1. *In situ* synthesis and assembly

In situ synthesis and assembly integrate the *in situ* generation and assembly of building blocks, making it particularly effective for constructing HOFs from species with limited solubility. For instance, Wu and Wasielewski *et al.* reported a one-pot synthesis and crystallisation strategy employing naphthalene diimide (NDI) or perylene diimide (PDI)—each functionalized with two terminal guanine units—as electron-accepting cores. The assembly of the G_2NDI and G_2PDI frameworks was initiated by *tert*-butyloxycarbonyl (Boc) deprotection using trifluoroacetic acid (TFA) in CH_2Cl_2, followed by vapor diffusion of MeOH into the TFA/CH_2Cl_2 solution at room temperature. This process produced rod-like crystalline morphologies, resulting in G-quadruplex frameworks with high thermal stability.[29] Similarly, during imidization, the molecular precursor (1,4,5,8-naphthalenetetracarboxylic dianhydride, NTCDA) spontaneously self-assembles into 2D HOF (HOF-DAT) nanosheets with a thickness of ~1 nm and lateral sizes up to 10 μm.[30]

2.2. *In situ* assembly

In situ assembly represents a powerful approach for nanostructure fabrication, achieved by controlling the assembling process of HOF precursors or integrating diverse composite components. This approach typically includes, solvothermal methods, electrospinning, and self-templated assembly (Fig. 2).

Solvothermal processing is a versatile strategy for the synthesis of HOFs at the nanoscale or nanocomposites (Fig. 2). This method leverages the inherent solution processability of HOF building blocks, allowing for precise control over crystal dimensions and morphologies by carefully modulating reaction parameters such as solvent polarity, temperature, and precursor concentration.[31] For instance, by adjusting solvent polarity and reaction conditions, Cao and Liu *et al.* showed that the dimensions of PFC-1 crystals could be precisely tailored from micrometres down to nanometres (*e.g.*, 100 × 300 nm).[14] Pushing the boundaries of dimensionality, Wang *et al.* employed a hydrothermal polycondensation to prepare graphitic carbon nitride-based quantum dots (CNQDs, ~2 nm). These units were then assembled *via* lateral hydrogen bonding into a porous, free-floating 2D film with an ultrathin thickness of approximately 2 nm.[32]

Electrospinning is a versatile and efficient technique that utilizes high-voltage electric fields to produce continuous fibres from polymer solutions. Li *et al.* fabricated antimicrobial nanofibers by electrospinning a precursor solution containing photoactive HOF building blocks and poly(vinylidene fluoride-*co*-hexafluoropropylene) (PVDF–HFP). During solvent evaporation, the polymer fibres solidified while simultaneously inducing the confined crystallisation of HOFs into uniform rod-like nanocrystals (~60 nm in length) embedded within the fibre matrix, rather than merely adhering to the surface.[33]

Self-templated assembly of HOFs can be used to synthesise nanostructured materials (Fig. 2). For instance, Yamauchi and Fujita *et al.* demonstrated the assembly of MA-BTC HOF nanowires from melamine (MA) and benzene-1,3,5-tricarboxylic acid (BTC). Crucially, these HOF nanowires acted as both a sacrificial template and a precursor. A subsequent solvothermal treatment with various metal salts directly transformed them into MOF nanotubes, faithfully replicating and retaining the initial tubular structure.[34]

2.3. Post conversion

Post-conversion involves transforming bulk materials into nanomaterials or integrating them with other substrates to form nanocomposites through subsequent physical or chemical processes, such as sonication, ball milling, electrophoretic deposition, solution casting, and post-synthesis (Fig. 2).

Sonication is a cost-effective and widely applicable post-conversion strategy for fabricating nano-HOFs or nanocomposites, particularly for exfoliation of bulk and layered HOFs into 2D H-bonded organic nanosheets (HONs) (Fig. 2). This method leverages mechanical energy to overcome the interlayer forces, yielding free-standing NSs or NRs that often retain the crystallinity and functionality of the parent material. White and Foster *et al.* exemplify the power of this approach by developing a top-down liquid exfoliation strategy for two-layered HOFs with a mild ultrasonic treatment (80 kHz, 12 h) in optimized solvents. This process produced highly stable, free-standing monolayer nanosheets (HON-1 and HON-2) with a uniform thickness of ~0.8 nm and lateral dimensions of several micrometres. The resulting HONs exhibited exceptional colloidal and structural stability, maintaining their crystalline monolayer structure even after rigorous treatment in hot water.[35]

Ball milling is an efficient, economical, and safe mechanical approach for exfoliating HOFs into nanosheets or downsizing the bulk material into nanoparticles, serving as an alternative to conventional sonication (Fig. 2). For example, Xiao and Luo *et al.* prepared a layered 2D HOF (HOFs-8) from N1, N3, N5-tris(pyridine-4-yl)benzene-1,3,5-tricarboxamide (TPBTC). The bulk crystalline material was successfully delaminated into ultrathin nanosheets (2–5 nm) through ball milling, thereby enhancing ion accessibility.[36] Beyond its use in post-conversion, mechanochemical synthesis also serves as a strategy for *in situ* assembly. Liu and Cao *et al.* demonstrated the versatility of mechanochemical synthesis by preparing eight structurally diverse nano-HOFs with predicted architectures, some of which are difficult to access *via* conventional solution-based methods. Notably, this approach enabled gram-scale production without loss of crystallinity, underscoring its potential to address a key scalability challenge in HOF fabrication. The strategy also facilitated the one-pot construction of functional composites; for instance, Pd@HOFs exhibited excellent catalytic activity toward CO oxidation.[37]

Solution casting is a technique that leverages the solution processability of HOFs to fabricate continuous crystalline thin films or nanofilm composites. Liu *et al.* demonstrated this method by dispersing bulk HOF-BTB crystals in *N*,*N*-dimethylformamide (DMF) to form a stable colloidal solution.[38] Cryo-electron microscopy (Cryo-EM) coupled with

three-dimensional electron diffraction (3D-ED) confirmed that the crystalline framework structure was preserved, with fragmented particles ranging from 20 to 200 nm. To fabricate the membrane, an anodic aluminum oxide (AAO) disk was immersed in the HOF-BTB casting solution at room temperature, followed by heating at 100 °C. Repeating this cycle yielded a continuous crystalline film with a thickness of approximately 126 nm. In contrast, membranes prepared *via in situ* assembly—by dissolving the BTB ligand directly in DMF—resulted in discontinuous and amorphous films. Moreover, this solution-based approach exhibits excellent substrate adaptability and generalizability to other HOF systems. Notably, Feng *et al.* first reported a microporous HOF membrane (UPC-HOF-6) grown on an Al_2O_3 substrate *via in situ* solution casting. This method promoted homogeneous nucleation and oriented crystal growth, achieving a polycrystalline membrane while its thickness is about 1 μm.[39]

Electrophoretic deposition (EPD) is a colloidal processing technique in which charged particles suspended in a liquid migrate under an electric field and deposit onto a conductive substrate to form uniform films or coatings. Liu and Cao *et al.* utilised the inherent negative surface charge of nano-PFC-1 crystals to achieve rapid EPD onto fluorine-doped tin oxide (FTO), forming dense, transparent electrochromic films (~500 nm) in just two minutes (Fig. 4C).[40] This approach was further used by Liu *et al.* for the fabrication of a heterostructured film by co-depositing PFC-45 and commercial Cu_2O particles onto carbon paper, illustrating the adaptability of this technique for designing multicomponent HOF–oxide electrodes.[41]

Post-synthesis stands as a highly effective chemical strategy for diversifying the functionality of nano-HOFs (Fig. 2), although it typically requires robust frameworks where strong H-bonding interactions preserve the crystalline integrity during chemical processing.[42] Zeng and Jiang *et al.* provided a compelling example of this strategy by constructing a robust biological HOF (HOF-25) from guanine-quadruplex building blocks, stabilized by Hoogsteen H-bonding within G-quartets and interlayer π–π stacking.[43] Benefiting from its exceptional stability across a wide pH range (7–11) and in common organic solvents, HOF-25 was further functionalized with Ni^{2+} ions. This post-synthetic metalation introduced positive charges into the neutral supramolecular layers without compromising the hydrogen-bonded network or crystallinity. The electrostatic modification weakened interlayer π–π interactions, facilitating subsequent exfoliation *via* sonication. The resulting HOF-25-Ni ultrathin nanosheets, with a uniform thickness of ~4.4 nm, were obtained in a yield of 56%—higher than that of the parent HOF-25 (45%). Post-chemical grafting can also be used to form HOF@polymers composites with core–shell structure. Du and Liu *et al.* reported an 'armour-plating' strategy where vinyl-terminated ionic liquids were grafted onto PFC-1 nanocrystals, followed by cross-linking polymerisation.[33] This process yielded polymer-grafted HOFs (PG-HOFs) with a well-defined core–shell architecture, featuring a HOF core protected by a dense polymer shell approximately 5.12 nm thick, significantly enhancing stability.

Beyond the typical methods introduced above, Wu and Jiang *et al.* demonstrated that annealing treatment is crucial for improving the homogeneity and stability of HOF membranes. They found that this process reconstructs the membrane's topology from a loose lamellar structure into a more compact one by removing water molecules from adjacent nanosheets. This structural transformation results in a thinner membrane (from 5.9 to 5.3 μm), leading to enhanced overall performance.[44]

3. Classification and fabrication of HOF nanomaterials

As molecular crystals, HOFs offer excellent solution processability, enabling their facile fabrication into nanostructures such as NSs and NRs. Their exceptional compatibility further allows integration into diverse composite materials. Accordingly, the HOFs discussed in this review can be categorized into two main classes: nanoscale HOFs and HOF-based nanocomposites. Based on their composition, the latter can be further divided into organic nanocomposites, organic–inorganic (hybrid) nanocomposites, and bio-nanocomposites (Fig. 1).

3.1. Nanoscale HOFs (nano-HOFs)

By modulating synthetic parameters and fabrication techniques, researchers have accessed a diverse library of nano-HOF architectures, ranging from zero-dimensional nanospheres to one-dimensional (1D) nanoribbons and two-dimensional (2D) nanosheets and nanofilms, with each morphology offering distinct advantages for specific applications.

Nanospheres & nanofibers. The key advantages of HOF nanospheres lie in their optimal size for enhanced mass transfer and cellular uptake, and good colloidal stability. Cowan and Cooper *et al.* demonstrated a solvent-dependent morphological control in the assembly of 2,6-bis(4-cyanophenyl)-4-(9-phenyl-9*H*-carbazol-3-yl)-pyridine-3,5-dicarbonitrile (CNP). Amorphous nanospheres were initially obtained *via* nanoprecipitation by injecting a THF solution into water under sonication. Surprisingly, increasing the THF/water ratio above 1/25 induced a gradual transformation into crystalline nanofibers over several days, with a faster transition (~30 min) observed at a 1/10 ratio.[45] This irreversible morphology switch from kinetic nanospheres to thermodynamic nanofibers is driven by π–π interactions. The implications of these morphological differences for photocatalysis will be addressed later.

Nanoribbons. HOF nanoribbons represent an intriguing morphological intermediate between nanosheets and nanorods, offering a unique combination of properties. Their thin thickness ensures short diffusion pathways, while their high aspect ratio provides continuous channels for directional charge or mass transport. Sun *et al.* successfully delaminated a bulk HOF in water to form stable, thin 1D porous nanoribbons (nr-HOF) using sonication. These nanoribbons had a thickness below 3 nm and lateral widths of ~100 nm, forming

a stable aqueous colloid. The resulting nanoribbons retain high crystallinity and porosity, which provides a fully exposed surface and strong adsorption capability. This accounts for their high loading capacity for doxorubicin (Doxo) (29.4%), substantially outperforming pristine bulk HOF, which exhibited only 16.5% loading under the same conditions.[46]

Nanosheets & nanofilms. HOF nanosheets have thin 2D layered architecture which maximizes the exposure of active sites and dramatically shortens diffusion pathways for guest molecules, leading to enhanced kinetics in catalysis and sensing applications.[35,47] Beyond nanosheets, Patel and Kushwaha *et al.* reported a family of free-standing HOF nano-thin films fabricated *via* a solution-based method at an air–liquid interface.[28,29] By employing a phenoxy-imine (PMAP) building block, the thickness of the resulting ^{CSMCRI}HOF-1 films could be precisely tuned—from approximately 40 nm to 1.2 μm—through systematic variation of the precursor concentration and reaction time. Notably, these thin films exhibited a significantly higher BET surface area (584.3 $m^2 g^{-1}$) than their bulk crystalline counterparts (329 $m^2 g^{-1}$), highlighting the benefits of nanoscale structuring.[47]

3.2. HOF organic nanocomposites

Beyond pristine nano-HOFs, bulk HOFs serve as versatile platforms for fabricating composites with organic materials like polymers, graphene oxide, HOFs and COFs.

HOF@polymers. The inherently organic nature of HOFs endows them with excellent compatibility with various polymer matrices, enabling the fabrication of diverse composite materials. A straightforward and widely adopted strategy involves the direct blending of HOF NPs with polymers. For instance, Huang *et al.* developed a HOF-30@PI mixed-matrix membrane by dispersing HOF-30 crystals into a polyimide (PI) matrix. The homogeneous dispersion of HOF particles without aggregation was attributed to H-bonding between the carbonyl groups of HOF-30 and the polymer, as well as their structural similarity (Fig. 3A).[48]

In addition to post-mixing, HOFs can be integrated during polymer formation. Liu *et al.* employed interfacial polymerisation to fabricate a thin film nanocomposite (TFN) membrane: an aqueous suspension of Nano-PFC-1 and piperazine (PIP) was coated onto a polyether sulfone (PES) substrate and reacted with 1,3,5-benzenetricarbonyl trichloride (TMC) to

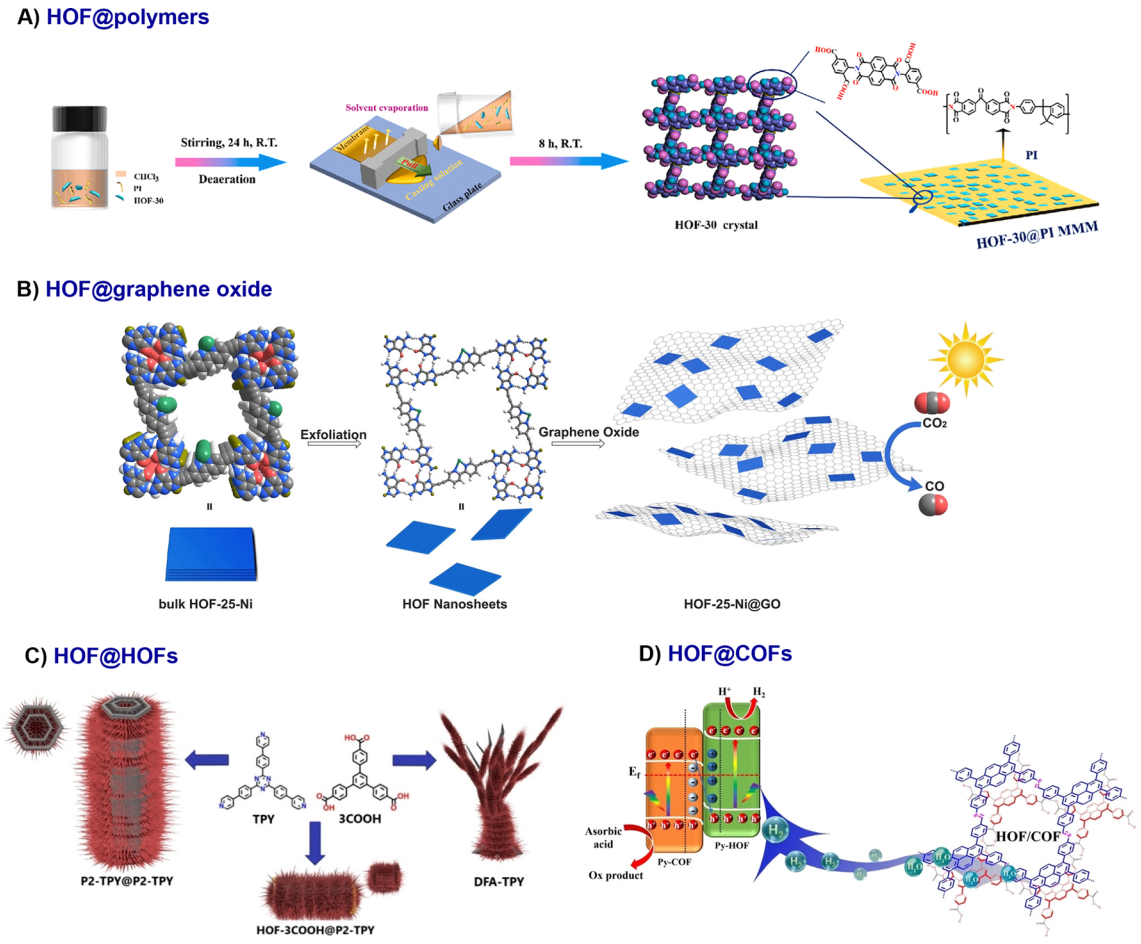

Fig. 3 Schematic diagram of the fabrication of HOF organic composites. A) HOF-30@PI MMMs[48] adapted with permission from ref. 48, Copyright 2021 Elsevier Inc; (B) HOF-25-Ni@GO,[43] adapted with permission from ref. 43, Copyright 2022 Wiley-VCH; (C) Hierarchical HOF-on-HOF superstructures constructed through controlled sequential crystallisation, adapted with permission from ref. 51, Copyright 2024 Wiley-VCH. (D) All-organic HOF/COF S-scheme heterojunction enabling efficient interfacial charge transfer,[52] adapted with permission from ref. 52, Copyright 2024 Wiley-VCH.

form a polyamide (PA) active layer embedded with uniformly dispersed HOF NPs.[49] In addition to nanofilms, nanofibers[48] and core–shell structures[33] were also observed as discussed in the fabrication section.

HOF@graphene oxide. Graphene oxide (GO) serves as an excellent substrate for constructing composite materials, in particular in the construction of electrical devices. Jiang and Zeng *et al.* formed an HOF@GO composites through an exfoliation-assisted assembly strategy, where HOF-25 was post-synthetically metalated with Ni(II) ions, then exfoliated into nanosheets *via* sonication and subsequently supported on GO to stabilize the nanosheets. The composites promote CO_2 reduction induced by visible light.[43] Han *et al.* demonstrated *in situ* assembly of a HOF@GO composite (denoted G-NDA-G) through an *in situ* synthesis and assembly strategy (Fig. 3B). The nucleophilic addition of DAT and 1,4,5,8-naphthalenetetracarboxylic dianhydride (NTCDA) generated building blocks that simultaneously formed H-bonded networks and π–π stacked with the GO substrate. This process yielded the H-NDA-G composite, which features 1D nanowires (~50 nm diameter) seamlessly integrated with GO sheets.[50]

HOF@HOFs. The pursuit of hierarchical crystals using HOFs as a platform represents an attractive concept with great potential for designing novel and promising materials with enhanced structural complexity and synergistic properties. Nevertheless, our group pioneered the 'HOF-on-HOF' concept in 2024 (Fig. 3C).[51] In this approach, pre-formed HOF-3COOH crystals served as the core and were subsequently immersed in a solution of a second pyridine-based precursor (TPY). Rapid solvent evaporation then induced the nucleation and growth of a dense shell of P2-TPY nanocrystals (100–200 nm) on the surface of the HOF-3COOH core, yielding a well-defined core–shell architecture. The success of this strategy relies on complementary hydrogen-bonding interactions between carboxyl and pyridine groups, combined with precise control over crystallisation kinetics and solvent evaporation rates. Notably, this approach enables precise tuning of surface wettability, enhancing the sorption performance of HOFs for the removal of water contaminants. This work establishes a facile route to expand the family of HOFs with integrated functionalities.

HOF@COFs. The integration of HOFs with COFs offers a powerful route to construct all-organic heterostructures due to their analogous 2D structural properties. A representative example was reported by Li and Zhang *et al.*, who developed a 2D/2D S-scheme heterojunction through a rapid solution dispersion method using pyrene-based HOF-H_4TBAPy (Py-HOF, PFC-1) and a pre-synthesized Py-COF (Fig. 3D). The two components self-assembled *via* H-bonding and π–π stacking, yielding a composite that retained high crystallinity and well-defined 2D morphology, along with a high BET surface area of 1516 $m^2\ g^{-1}$. More importantly, the heterojunction exhibited enhanced light absorption, reduced bandgap, and markedly improved charge separation efficiency, collectively contributing to its good photocatalytic activity.[52] By replacing 2D COFs with their analogous carbon nitride, Yu and Chen *et al.* constructed a Z-scheme heterojunction (PFC-1/CNNS) between a HOF (PFC-1) and carbon nitride nanosheets (CNNS) by dispersing CNNS in a DMF solution of the H_4TCBP linker, followed by the solvent-induced crystallisation of PFC-1 on the CNNS surface. This method resulted in PFC-1 nanorods growing intimately on the CNNS with strong interfacial electronic interaction and charge transfer capability as revealed by the binding energy shifts for key elements.[53]

3.3. HOF organic–inorganic nanocomposites

The integration of metal species with HOFs enables the construction of functional organic–inorganic hybrid nanomaterials. These strategies not only modulate the morphology and porosity of HOF materials but also introduce highly active metal sites for electrocatalysis and energy storage.

HOF@M^{n+}. *In situ* coordination can drive structural evolution without pyrolysis. Wang and Xu *et al.* introduced Ag^+ ions into the cyanuric acid–melamine (CAM) framework, where the formation of Ag–N bonds triggered a crystal transformation from nanorods to chain-like nanofibers (Fig. 4A). These fibres self-assembled into a free-standing CAM-Ag membrane, demonstrating the potential of metal coordination to reconfigure HOF morphology and enable flexible device integration.[54]

HOF@M_xO_y. The integration of HOFs with metal oxides (M_xO_y) offers a versatile route to create composite architectures, including core–shell structures[55] and crystalline thin films,[38,40,41,56] with enhanced interfacial properties. A representative blending strategy was demonstrated in the synthesis of HOF@TiO_2 composites, where pre-formed HOF-TCPB-373 sheets were uniformly mixed with TiO_2 NPs in aqueous suspension (Fig. 4B).[55] Driven by H-bonding or coordination between surface hydroxyl groups on TiO_2 and carboxyl groups in the HOF, the flexible HOF sheets partially wrapped the oxide particles. This interfacial interaction resulted in a more negative zeta potential and enhanced hydrophilicity (water contact angle 40%TiO_2@HOF, 51°) compared to the individual components (TiO_2, 105°), highlighting the role of HOFs in modulating surface properties.

HOF@NPs. Employing HOFs as a support matrix for functional nanoparticles represents a promising strategy for engineering composite materials with enhanced and often synergistic, properties. The resulting composites generally adopt one of three configurations: core–shell structures (HOF shell), NPs confined within the HOF pores and surface-supported NPs. For core–shell structures, a representative stepwise approach was demonstrated by Liu *et al.*, who constructed core–shell UCNPs@PFC-55 nanostructures for near-infrared (NIR)-responsive antibacterial applications (Fig. 4C). Oleate-capped upconversion NPs (UCNPs, β-$NaYF_4$:Yb,Er, ~36 nm) were first functionalized with PDI-C ligands, followed by heterogeneous nucleation of PFC-55 to form a uniform ~6 nm HOF shell.[57] The resulting composite exhibited efficient resonance energy transfer (RET) from the UCNP core to the HOF shell, with an RET efficiency of up to 83.9%, enabling effective NIR-driven bacterial inhibition. The generalizability of the modular strategy was further validated using other HOFs such as PFC-73-Ni.[58] Similarly, Li and Chen *et al.* developed a

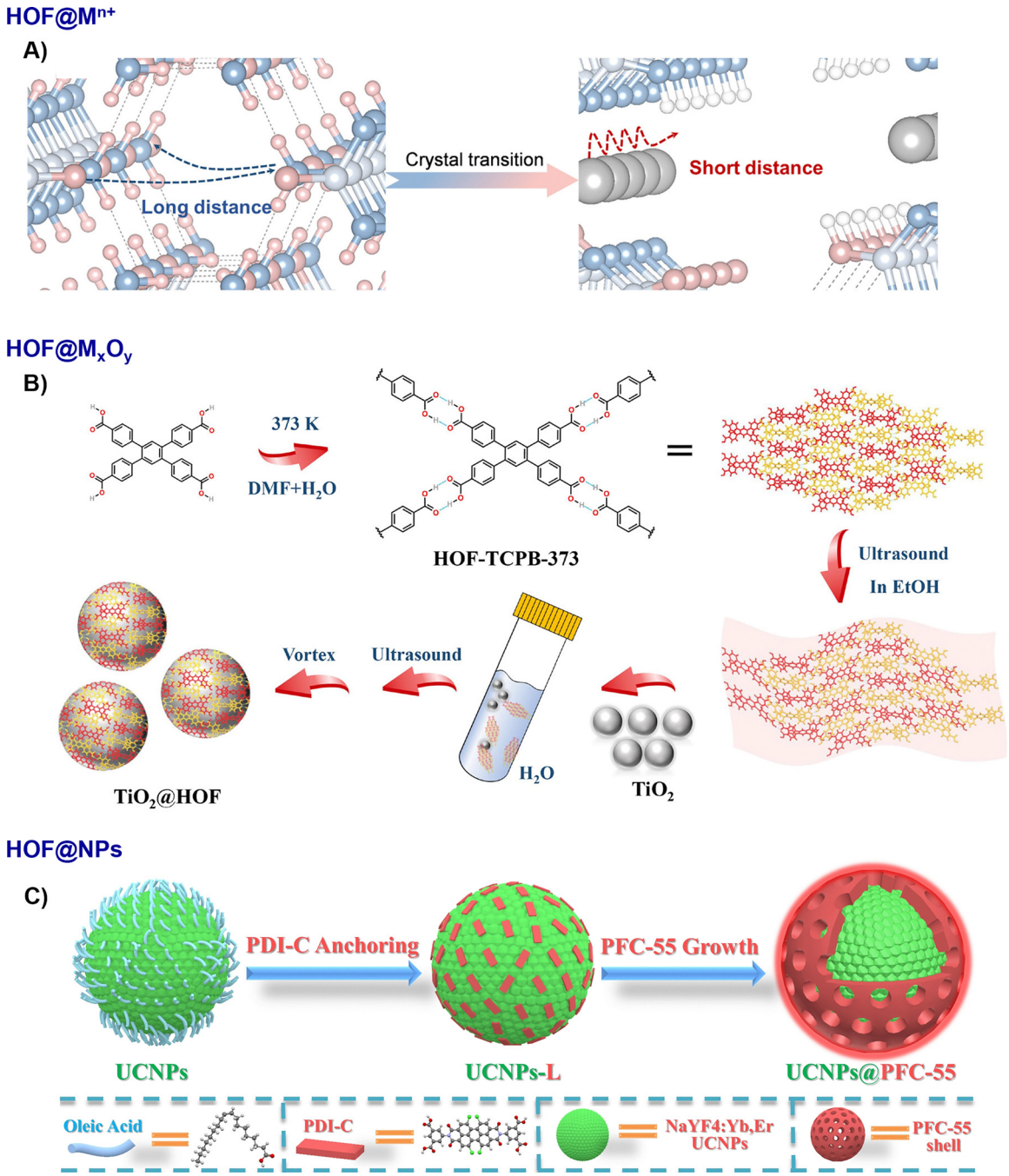

Fig. 4 Schematic diagram of the fabrication of HOF organic–inorganic composites. (A) CAM-Ag, adapted with permission from ref. 54, Copyright 2025 Wiley-VCH; (B) HOF-25-Ni@GO45, adapted with permission from ref. 55, Copyright 2023 Elsevier Inc; (C) UCNP@PFC-55,[57] adapted with permission from ref. 57, Copyright 2021 Wiley-VCH.

ratiometric fluorescence sensor by *in situ* growing HOF-101 around pre-synthesised Pt_2Cu_4 metal nanoclusters (MNCs, ~2 nm). Guided by favourable electrostatic interactions, the MNCs were uniformly encapsulated within the HOF matrix, forming the Pt_2Cu_4@HOF-101 composite with well-preserved luminescence properties.[59] In a composite electrode design, Chen and Zhang *et al.* grew HOF-FJU-1 *in situ* on Ru-decorated carbon nanotubes, forming a core–shell HOF-FJU-1-Ru@CNT structure that enhanced electrolyte wettability and interfacial ion transport in lithium–sulphur batteries.[60] *In situ* methods provide an alternative route to achieve highly dispersed NPs within HOF matrices. Zhu *et al.* fabricated a HOF–sulphide composite (MTC@$Co_{1-x}Fe_xS_2$) through a two-step hydrothermal process, where bimetallic $Co_{1-x}Fe_xS_2$ NPs were grown within a melamine–trithiocyanurate (MTC) HOF, resulting in a uniformly integrated electrocatalyst.[61]

For NPs confined within the HOF pores, Li and Farha *et al.* developed an *in situ* photo-deposition method to fabricate AgNPs@HOFs, where UV irradiation of a mixture containing HOF building blocks and $AgNO_3$ led to the formation of ultra-small silver NPs ($\sim$1 nm) uniformly distributed within the HOF pores. In contrast, conventional deposition onto pre-formed HOFs typically yielded larger AgNPs (10–20 nm) on the external surface, highlighting the potential of the *in situ* approach for achieving fine dispersion.[62] For the last type configuration, Liu and Cao *et al.* reported a one-pot photochemical strategy that simultaneously reduced Ag^+ ions to form Ag NPs ($\sim$5 nm) on a HOF surface while oxidising the HOF framework to its radical form (Ag@oxHOFs), demonstrating the potential for concurrent nanoparticle formation and framework modification.[63]

3.4. HOF biocomposites

The inherent metal-free skeleton and excellent biocompatibility of HOFs position them as components for constructing functional biocomposites, particularly with enzymes and other biomolecules. Through co-crystallisation and biomaterial integration, HOF-based biocomposites offer new opportunities in biocatalysis, biosensing, biomedicine, and sustainable material design.

HOF@enzyme. While the pore size of HOFs ($<$5 nm) generally precludes post-synthetic enzyme encapsulation, this limitation has been overcome through co-crystallisation strategies that enable precise and uniform biomolecule integration during framework assembly. A landmark study by Falcaro and Doonan *et al.* established a mild, one-pot aqueous synthesis for encapsulating enzymes within the water-stable BioHOF-1 at room temperature (Fig. 5A). By mixing enzyme solutions with ionic building blocks in a specific sequence, the framework crystallised directly around the biomolecules, yielding composites with high crystallinity, uniform enzyme distribution, and exceptional stability across a broad pH range (5–10), including polar organic solvents and phosphate buffers—conditions where many MOFs (*e.g.*, ZIF-8) decompose.[15] This co-crystallisation protocol, systematically detailed by Ouyang *et al.*,[64] has enabled diverse applications, including the co-encapsulation of glucose oxidase (GOx) and catalase (CAT) within HOF-101 (denoted EnHOF-101) for enhanced cascade catalysis (Fig. 5B).[65–71] Further extending this concept, Tang *et al.* developed a tri-enzyme system (β-galactosidase-GOx-HRP) confined within MHOF-101, confirmed by confocal laser scanning microscopy, with a uniform spatial distribution within mesopores rather than surface adsorption.[72] More complex bio-interfaces have also been realised, such as the light-driven nanoreactor constructed by Yang *et al.* through interfacing HOF (TBAP-α) with engineered α-carboxysome shells encapsulating [FeFe]-hydrogenases.[73]

HOF@biopolymers. Beyond acting as a shell, HOFs have been integrated with macroscopic biomaterials to form membrane composites. Jiang and Zhang *et al.* utilised bacterial cellulose (BC) as a structural scaffold to expand the interlayer spacing of HOF-H_4TCPB, forming a fibrous HOF-H_4TCPB/BC composite membrane with expanded nanochannels that significantly enhanced water adsorption/desorption kinetics (Fig. 5C).[74] In another approach, Li and Farha *et al.* fabricated a fibre composite by drop-casting a suspension of stable mesoporous HOF-102 onto cotton, realising the efficient photochemical detoxification of a mustard gas simulant.[75]

4. Applications

4.1. Separation

HOF nanomaterials have demonstrated significant potential in separation applications, including gaseous, aqueous, and radionuclide capture processes. Their tuneable pore architectures, framework flexibility, and rich surface chemistry enable precise molecular recognition and selective transport.

HOF-based membranes exhibit exceptional gas separation performance, often attributed to their unique structural responsiveness. Huang *et al.* demonstrated this by incorporating flexible HOF-30 into a PI matrix to fabricate a mixed-matrix membrane (MMM) (Fig. 6A–C).[48] This integration yielded a HOF-30@PI MMM with a 10 wt% loading, which exhibited a high H_2 permeability of 428.1 barer and an H_2/CH_4 separation factor of 61.7. This value is approximately 7.6 times higher than that of the pure PI membrane. Furthermore, the HOF-30@PI MMM displayed pressure-regulated H_2/CH_4 separation performance, a behaviour arising from the local dynamics of the flexible HOF structure. The potential of nano-HOF membranes was further demonstrated by the HOF-BTB@AAO system, which achieved high propylene/propane separation performance (C_3H_6 permeance $\sim$200 GPU, separation factor 14) *via* a molecular sieving mechanism.[38] Beyond membrane separations, HOF nanocrystals also excel as adsorbents for gas purification. Janiak *et al.* reported a nanocrystalline CB6–H material with exceptional SO_2 uptake capacity (6.18 mmol g^{-1} at 273 K) and selectivity over CO_2 (IAST $\approx$ 120–142), ranking among the highest-performing organic porous materials for fluent gas desulfurization (Fig. 6D and E).[31]

In liquid phase separations, HOF-based membranes show promise for water purification and resource recovery. The first demonstration of HOFs in liquid separation came from a thin film nanocomposite membrane (HOF-TFN-2) incorporating Nano-PFC-1 NPs within a polyamide layer. This membrane achieved high permeability and excellent dye rejection ($>$97% for rhodamine B, $>$95% for Congo red and Coomassie brilliant blue, $>$92% for calcein, and $\sim$84% for methyl blue) through precise molecular sieving.[49] The inherent selectivity of HOFs has also been leveraged for strategic applications beyond simple separation. For instance, JZS-1, a porphyrin-based HOFs, exhibited preferential adsorption for cationic dyes in mixtures containing cationic methylene blue (MB^+) along with either neutral or anionic dyes, despite not being designed for molecular separation. This adsorption property was leveraged to construct a host–guest system (MB@JZS-1), in which Förster resonance energy transfer (FRET) from the framework to the encapsulated MB significantly enhanced singlet oxygen generation. As a result, the material achieved good antimicrobial

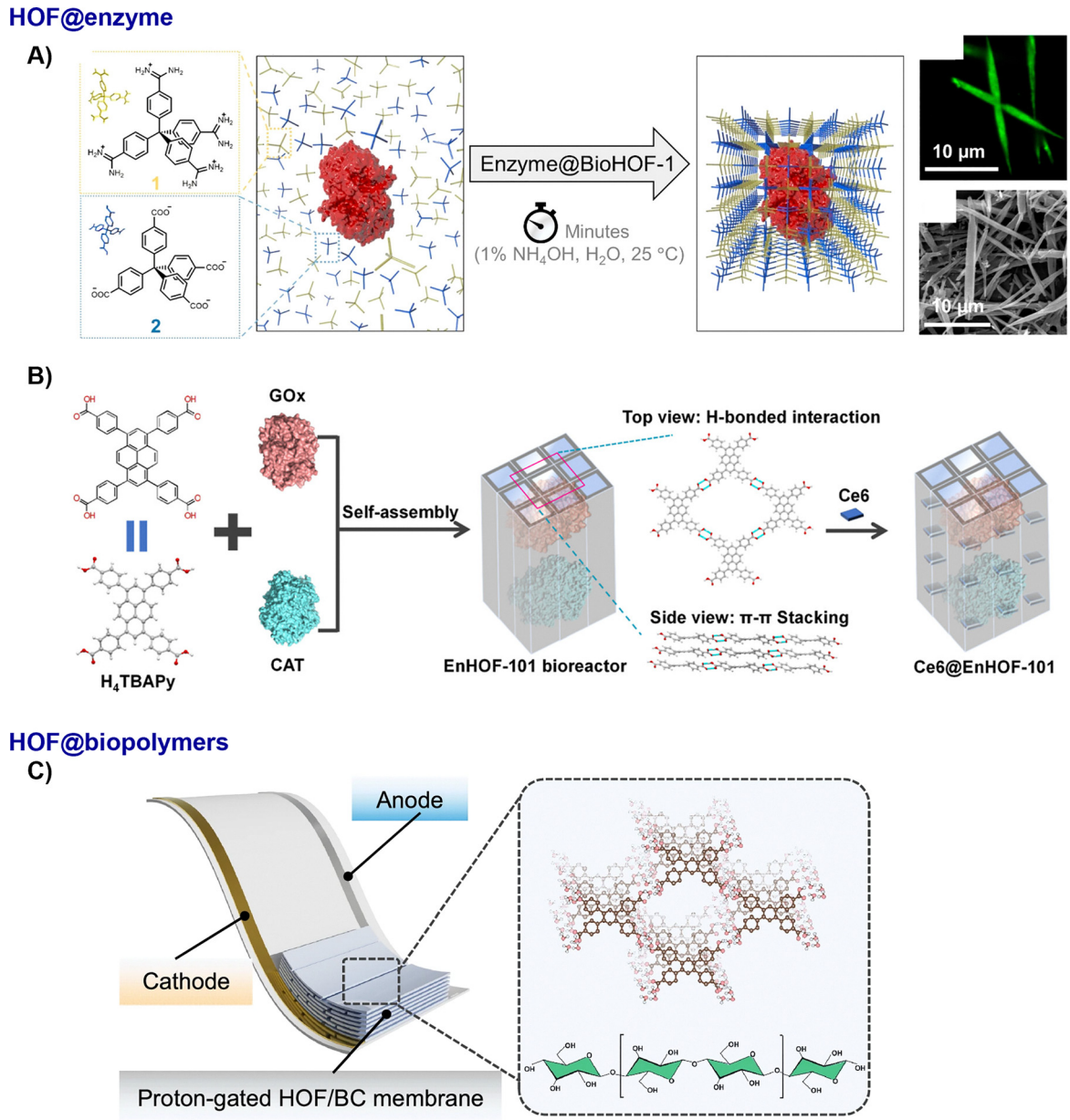

Fig. 5 Schematic diagram of the fabrication of HOF biocomposites. (A) BioHOF-1,[15] adapted with permission from ref. 15, Copyright 2019 ACS; (B) photobiocatalytic cascade nanoreactor Ce6@EnHOF-101,[65] adapted with permission from ref. 65, Copyright 2022 ACS; (C) proton-gated HOF/BC membrane,[74] adapted with permission from ref. 74, Copyright 2025 Springer Nature.

performance, with 99.9% inhibition of *Staphylococcus aureus* under red light irradiation.[76]

In addition to conventional molecular separation, HOF nanomaterials demonstrate exceptional capability in capturing valuable or hazardous elements. ^{CSMRI}HOF-1 film achieved a notable uranium extraction capacity of 17.9 mg g^{-1} from natural seawater over 30 days.[47] Liu and Du *et al.* fabricated PG-HOFs that set new benchmarks for radioactive anion capture, with capacities of 699.0 mg g^{-1} for I^- and 1.616 g g^{-1} for ReO_4^- (a TcO_4^- surrogate). PG-HOFs exhibited fast kinetics (>98% removal in 45 seconds), excellent selectivity, wide pH tolerance (3–13), and exceptional reusability over 30 cycles.[77]

4.2. Catalysis

HOFs have emerged as a versatile platform for designing advanced catalytic materials, and their based nanomaterials have demonstrated notable performance across diverse reaction systems, such as oxygen evolution reaction (OER), hydrogen evolution reaction (HER), CO_2 conversion, environmental catalysis, and biocatalysis, *etc*.

Oxygen evolution reaction. OER is a crucial electrochemical process involving a multi-step electron transfer for the oxidation of water to molecular oxygen, which is central to renewable energy technologies like water electrolysis. HOFs might serve as excellent matrix for fabricating metal-based electrocatalysts.[57]

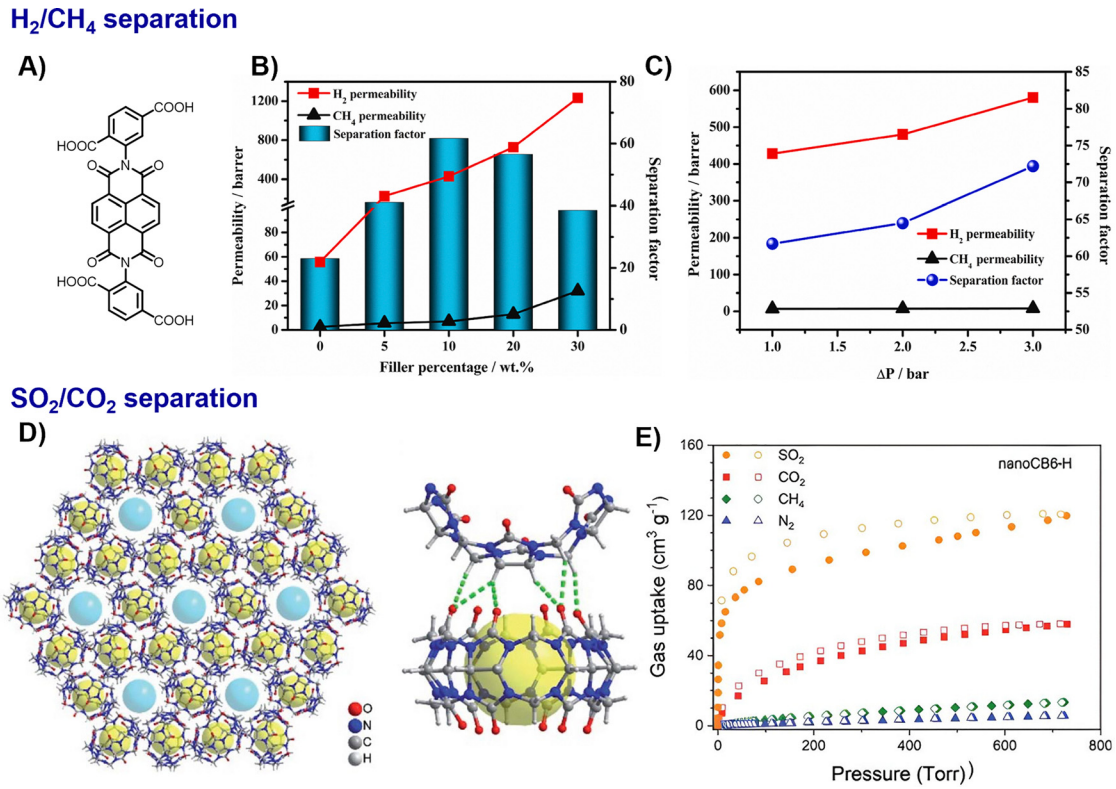

Fig. 6 Properties of HOF-30 MMMs:[48] (A) molecular building block, (B) permeability and separation factor of the HOF-30 MMMs with different HOF-30 loadings at 1 bar and 25 °C. (C) The H_2/CH_4 separation performance of HOF-30@PI MMM with 10 wt% HOF-30 loading at different pressure difference (ΔP), adapted with permission from ref.48, Copyright 2021 Elsevier B.V.; CB6-H used for SO_2/CO_2 separation:[31] (D) view of the honeycomb-like structure of CB6-H along the *c*-axis and the intermolecular hydrogen bonds between neighbouring CB6 molecules, (E) single gas sorption isotherms measured for recycled nanoCB6-H at 293 K, adapted with permission from ref. 31, Copyright 2019 RSC.

Zhu *et al.* integrated bimetallic sulphide NPs ($Co_{1-x}Fe_xS_2$) within an HOF, achieving an OER overpotential of 130 mV at a high current density of 100 mA cm^{-2} and durability over 16 hours and 2000 cycles, significantly outperforming commercial IrO_2. This enhanced activity stems from a synergistic effect where the HOF matrix ensures nanoparticle dispersion and improves conductivity, while the sulphides provide abundant active sites (Fig. 7).[61]

Hydrogen evolution reaction. HER is a two-electron transfer electrochemical process that occurs at the cathode, reducing protons or water molecules to generate gaseous hydrogen, and is a key reaction for sustainable hydrogen production. Extensive research has focused on employing porous materials as supports for noble metal catalysts in the HER. For instance, MOFs have demonstrated that incorporating metal-active sites can significantly boost catalytic performance.[78] Extending this concept beyond MOFs, metal-free HOFs and HOF-based heterojunctions have also demonstrated promising activity for the HER. Giri *et al.* developed a series of metal-free HOFs, revealing that sulfur-integrated frameworks like B.TC can act as efficient HER electrocatalysts in acid, achieving an overpotential of 290 mV at 10 mA cm^{-2}. This could be attributed to the simultaneous H-adsorption at C and S sites.[79] Heterojunction is also an effective strategy to improve the charge separation process. The all-organic Z-scheme heterojunction, PFC-1/CNNS, was constructed by integrating a HOF (PFC-1) with g-C_3N_4 nanosheets (Fig. 8A and B). This hybridization altered the surface wettability, reducing the water contact angle from 80° to 0°. Importantly, the PFC-1/CNNS heterojunction exhibited an enhanced photocatalytic HER rate of 4450 μmol h^{-1} g^{-1} under visible light ($\lambda > 420$ nm), marking an 11-fold enhancement over pristine g-C_3N_4. This work highlights the role of HOFs in enhancing hydrophilicity and stability of the hybrid material, addressing common limitations of g-C_3N_4-based catalysts, such as poor wettability.[53] This concept was advanced further with the first report of an S-scheme HOF/COF heterojunction (Fig. 8C–E). The Py-HOF/Py-COF heterostructure exhibited a high HER rate of 390.68 mmol g^{-1} h^{-1} with an apparent quantum yield (AQY) of 61.35% at 450 nm, representing enhancements of 2.28-fold and 9.24-fold relative to pristine Py-HOF and Py-COF, respectively. This exceptional performance is attributed to the well-matched interfaces between the two semiconductors, where π–π interactions facilitate the formation of a face-to-face closely connected heterojunction. Such a configuration not only provides abundant active sites but also strengthens the built-in electric field, thereby promoting efficient S-scheme charge transfer.[52] Cooper and Liu *et al.* constructed a hybrid biosystem, H–S/TBAP-α, achieving visible-light-driven sacrificial hydrogen production with a rate of 3.97 mmol g^{-1} h^{-1}, nearly five times higher than TBAP-α

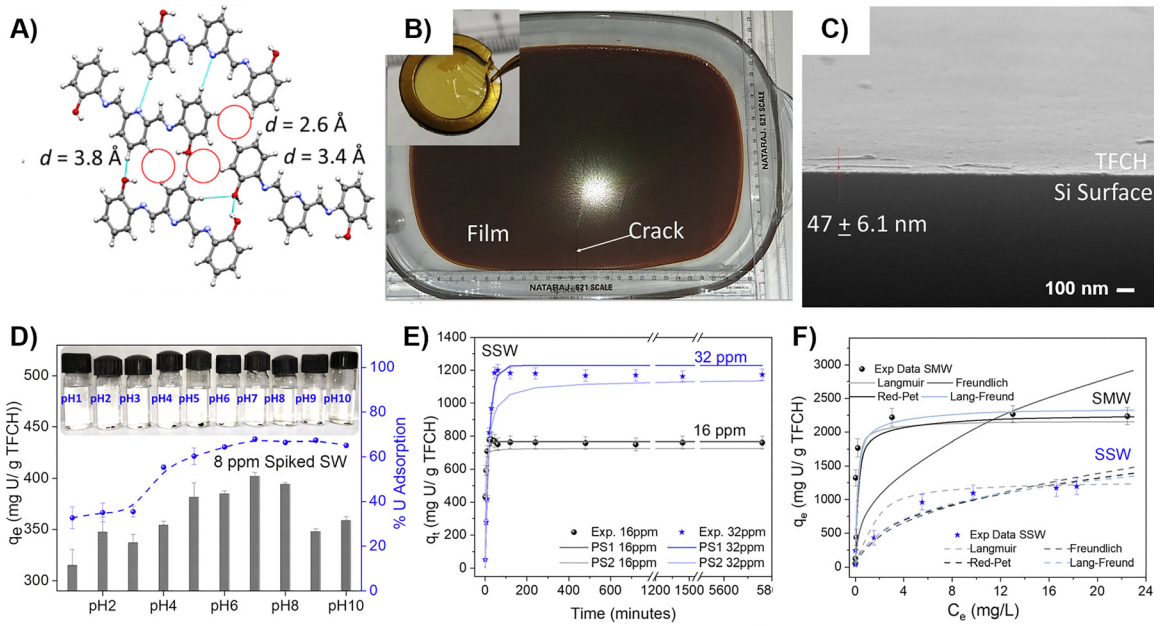

Fig. 7 Large-area free-standing thin film of ^{CSMCRI}HOF-1, the TFCH, its characterization and adsorption experiments[47] (A) crystal structure of ^{CSMCRI}HOF-1, (B) scalable preparation of TFCH, (C) cross-section SEM image of TFCH on Si wafer, (D) uranium uptake under different pH conditions, (E) adsorption kinetics of TFCH in 16 and 32 ppm spiked seawater, (F) adsorption isotherms with varied initial concentrations of uranium, adapted with permission from ref. 47, Copyright 2022 Elsevier Inc.

alone.[73] A pioneering work by Yang and Cowan *et al.* discovered that the morphology can switch the photocatalytic activity between HER and ORR(Fig. 8F–I). The study on CNP polymorphs revealed that fibre polymorph (CNP-f) favoured H_2 evolution (31.85 mmol g^{-1} h^{-1} under solar simulation), while another spherical solid (CNP-s) selectively produced H_2O_2 (3.20 mmol g^{-1} h^{-1} under O_2), a phenomenon governed by differences in excited-state delocalisation induced by packing. This highlights the profound impact of nanoscale morphology on catalytic function from a single molecular building block.[45] Beyond structural design, Zhu *et al.* explored the photophysical processes in HOF-H_4TBAPy (PFC-1) and identified a micropore-confined exciton transfer mechanism, wherein excitons undergo ultrafast migration to the pore walls prior to dissociation, thereby drastically reducing recombination (Fig. 9).[80] Through morphological studies, they observed that increasing the 1D channel length led to photoactivity that initially remained stable before declining in an approximately inverse proportional manner. Conversely, a decrease in the average material length resulted in a reduction of the water contact angle from 34.50° to 11.85°, reflecting enhanced surface hydrophilicity. By optimizing the channel length to ≤590 nm, a high HER rate of 358 mmol h^{-1} g^{-1} was attained, highlighting the pivotal role of morphology control in both exciton management and surface affinity regulation.

CO_2 conversion. The conversion of CO_2 into valuable fuels using sunlight or electricity is a critical challenge. A pioneering example is HOF-25-Re, which was constructed by post-metalating a biological G-quadruplex motif with Re complexes. This system achieved a CO production rate of 1448 μmol g^{-1} h^{-1} with 93% selectivity and an eight-fold higher turnover number, significantly outperforming its homogeneous analogue (Fig. 10A–C).[81] Building up on this, HOF-25-Ni@GO achieved a photocatalytic CO production rate of 24 323 μmol g^{-1} h^{-1} with 96.3% selectivity, among the highest for porous organic catalysts. The enhanced performance can be attributed to increased active site accessibility and facilitated electron transfer *via* the nanoscale engineering, where a HOF was exfoliated into ultrathin nanosheets hosting atomically dispersed Ni sites and supported on graphene oxide.[43] A significant advancement toward practical application is the development of photocatalysts that operate without sacrificial agents. The PFC-45/Cu_2O@CP film achieved a CO production rate of 11.81 μmol g^{-1} h^{-1} in pure water with nearly 100% selectivity. This performance was 2.4 and 3.2 times higher than that of PFC-45@CP and the bulk PFC-45/Cu_2O, respectively. These results highlight the dual benefit of the heterojunction film architecture in promoting charge separation and scalability (Fig. 10D–G).[41]

Environmental catalysis. An attractive trend in HOF research is the design of multifunctional systems that combine adsorption, catalysis, and even autonomous motion for advanced environmental remediation. Li and Jiang *et al.* developed a TiO_2@HOF heterojunction structure to combine high adsorption capacity with photocatalytic degradation for water purification. TiO_2@HOF concentrates pollutants (Rhodamine B) near the photocatalytic TiO_2 sites, leading to a 99% removal efficiency, combining 30% adsorption with 69% photodegradation.[55] Li and Lu *et al.* constructed a tri-functional system (HOF@Fe^{3+}) by integrating selective adsorption,

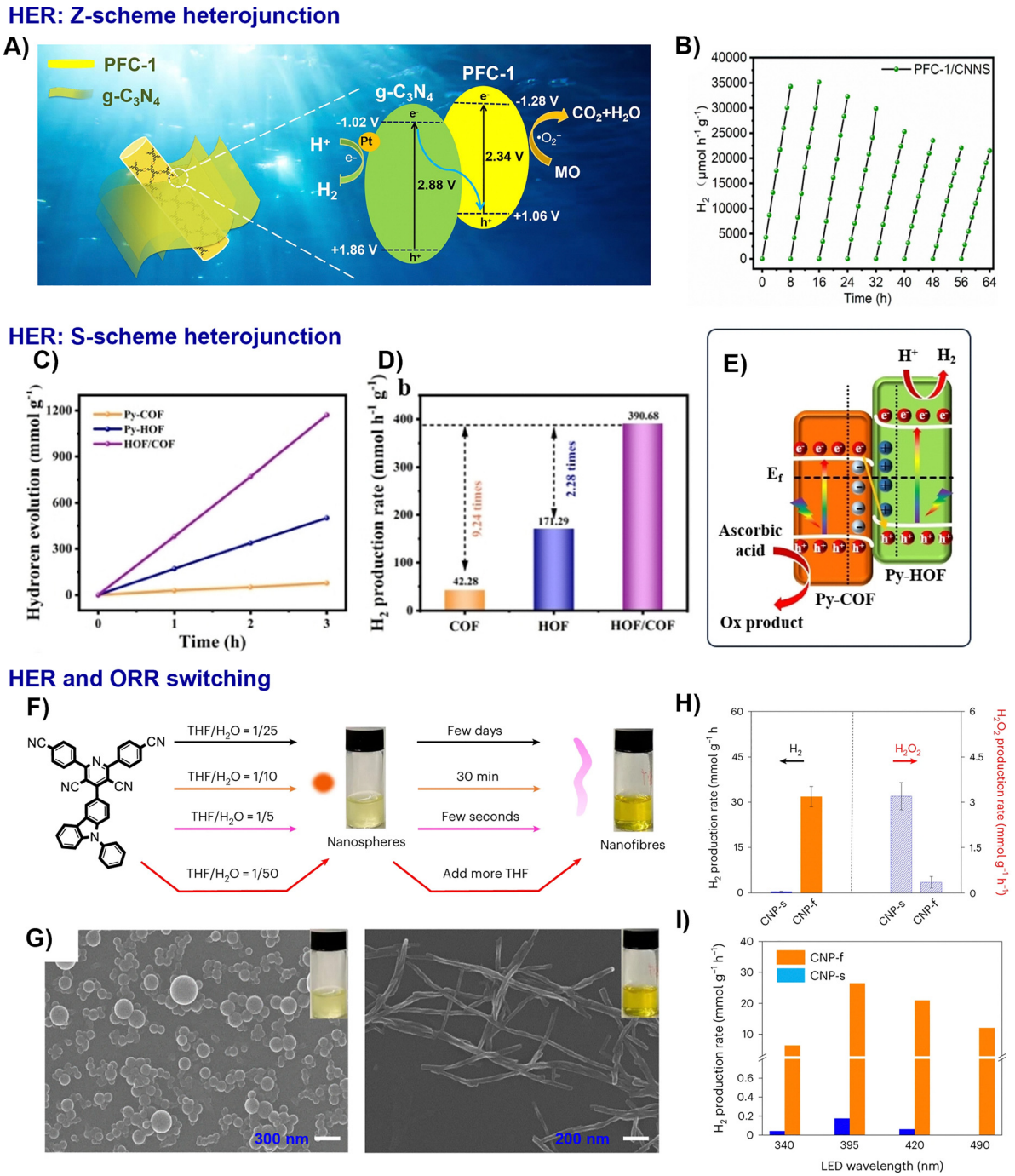

Fig. 8 Representative examples of nano-HOFs and its composites used in HER: PFC-1/CNNS heterojunction system,[53] (A) proposed carrier separation and photocatalytic processes under visible light, (B) HER cycling stability of PFC-1/CNNS, adapted with permission from ref. 53, Copyright 2022 Elsevier Inc; HOF/COF:[52] (C) time profiles of photocatalytic hydrogen generation, (D) average hydrogen evolution rate, (E) photocatalytic reaction mechanism of S-scheme heterojunction, adapted with permission from ref. 52, Copyright 2024 Wiley-VCH. CNP,[45] (F) summary of the morphology transformation, (G) SEM images of CNP-s and CNP-f, (H) photocatalytic H_2 and H_2O_2 production, (I) photocatalytic H_2 production, adapted with permission from ref. 45, Copyright 2023 Springer Nature.

photodegradation, and photocatalytic hydrogen production (Fig. 11A and B). It achieved a notable adsorption capacity for pollutants such as bisphenol A (452 mg g^{-1}) and enabled its complete degradation within 20 minutes. The same material also exhibited a high HER rate (21.55 mmol g^{-1} h^{-1}) using Fe^{3+} as a non-noble metal cocatalyst. The system's efficiency stems from the HOF's porous structure and the Fe^{3+}/Fe^{2+} redox cycle, which promotes charge separation for both oxidative degradation and reductive proton reduction.[82] Beyond static materials, HOFs can be engineered into dynamic, self-propelled systems.

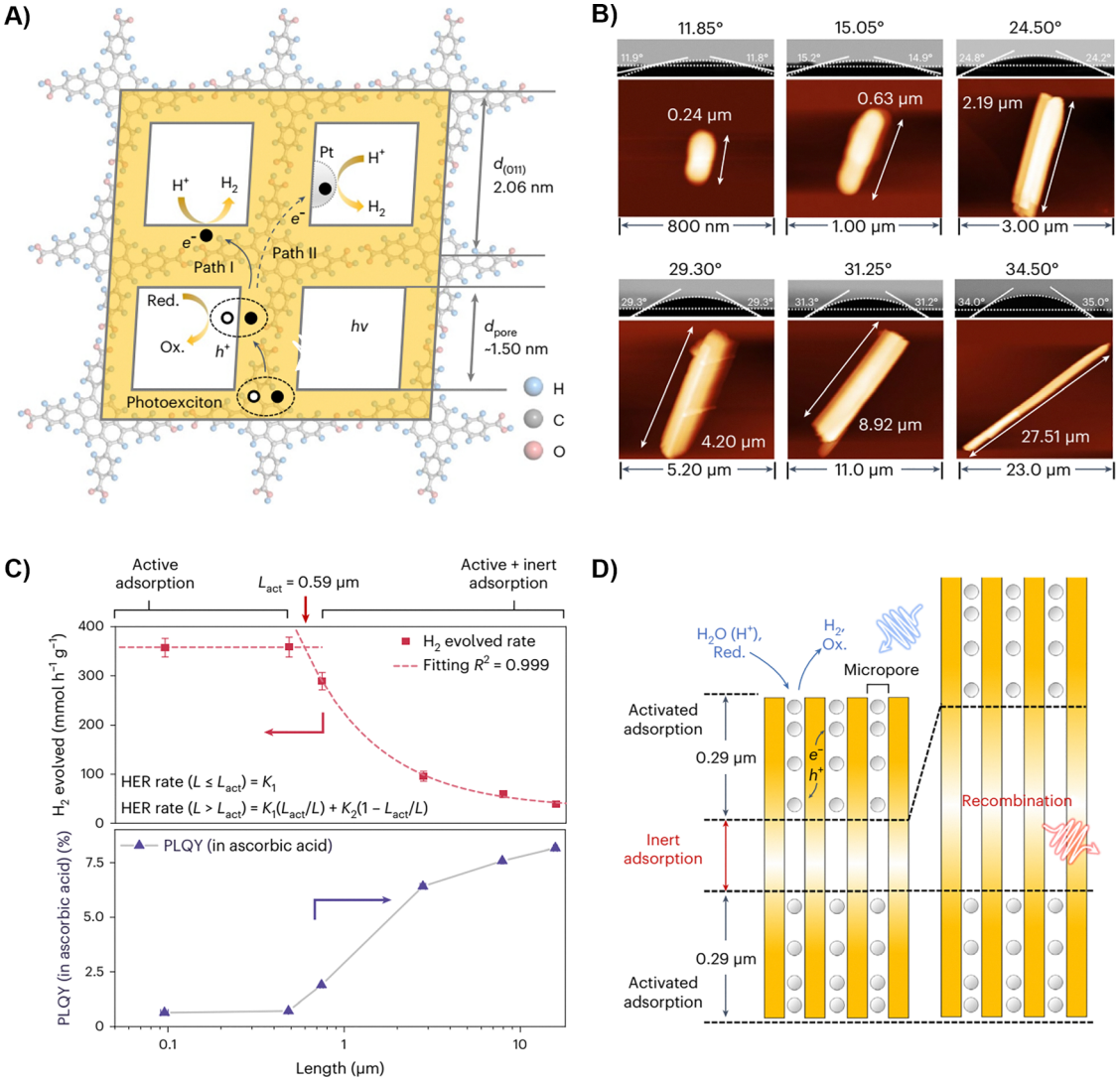

Fig. 9 Micropore-confined exciton transfer in HOFs.[80] (A) Schematic illustration of the possible migration behavior of excitons in the microporous framework. (Red.: reducing agent and Ox.: oxidation product.), (B) atomic force microscopy images of HOF-H4TBAPy nanorods of different lengths and their corresponding contact angles with water, (C) plot of maximum H_2 evolution rate as a function of the mean length of the 1D microporous channel of the samples and the relationship between PLQY in ascorbic acid and different 1D channel lengths, (D) schematic diagram of HOF-H4TBAPy adsorbing water and hole scavenger. The length of the active adsorption region at both ends was determined to be 0.30 μm. Adapted with permission from ref. 80, Copyright 2023 Springer Nature.

A key innovation is the enzyme-driven micromotor (CAT@HOF), where CAT encapsulated within a mesoporous HOF shell decomposes H_2O_2 fuel into O_2 bubbles for propulsion (Fig. 11C–E).[67] This self-propulsion, achieving speeds up to 8.07 μm s^{-1}, enhances mixing and interaction with pollutants giving a more efficient degradation.

Biocatalysis. The encapsulation of enzymes and functional proteins within HOFs has emerged as a powerful strategy to enhance their stability and unlock new therapeutic capabilities. Moving beyond traditional MOFs, HOFs offer excellent biocompatibility and unique modes of interaction with biomolecules, leading to a progression from simple protection to sophisticated intracellular biorthogonal catalysis. In 2019, Falcaro and Doonan *et al.* published a pioneering work to prove that enzymes like catalase and alcohol oxidase could be encapsulated in BioHOF-1 while retaining high activity under harsh conditions (*e.g.*, 60 °C, urea), outperforming MOF encapsulants such as ZIF-8 analogues (Fig. 12A–C). This work demonstrates the potential of employing HOFs as a metal-free, biocompatible, and synthetically tuneable platform for enzyme stabilisation.[15] This concept was expanded by creating H-bonded biohybrid frameworks (HBFs), which leverage universal protein surface residues to drive framework formation. This method bypassed complex protein engineering, yielding bioreactors with improved recyclability and stability against proteolysis compared to ZIFs.[71]

The excellent biocompatibility of HOFs enables their use for intracellular enzyme delivery. TA-HOFs were shown to deliver

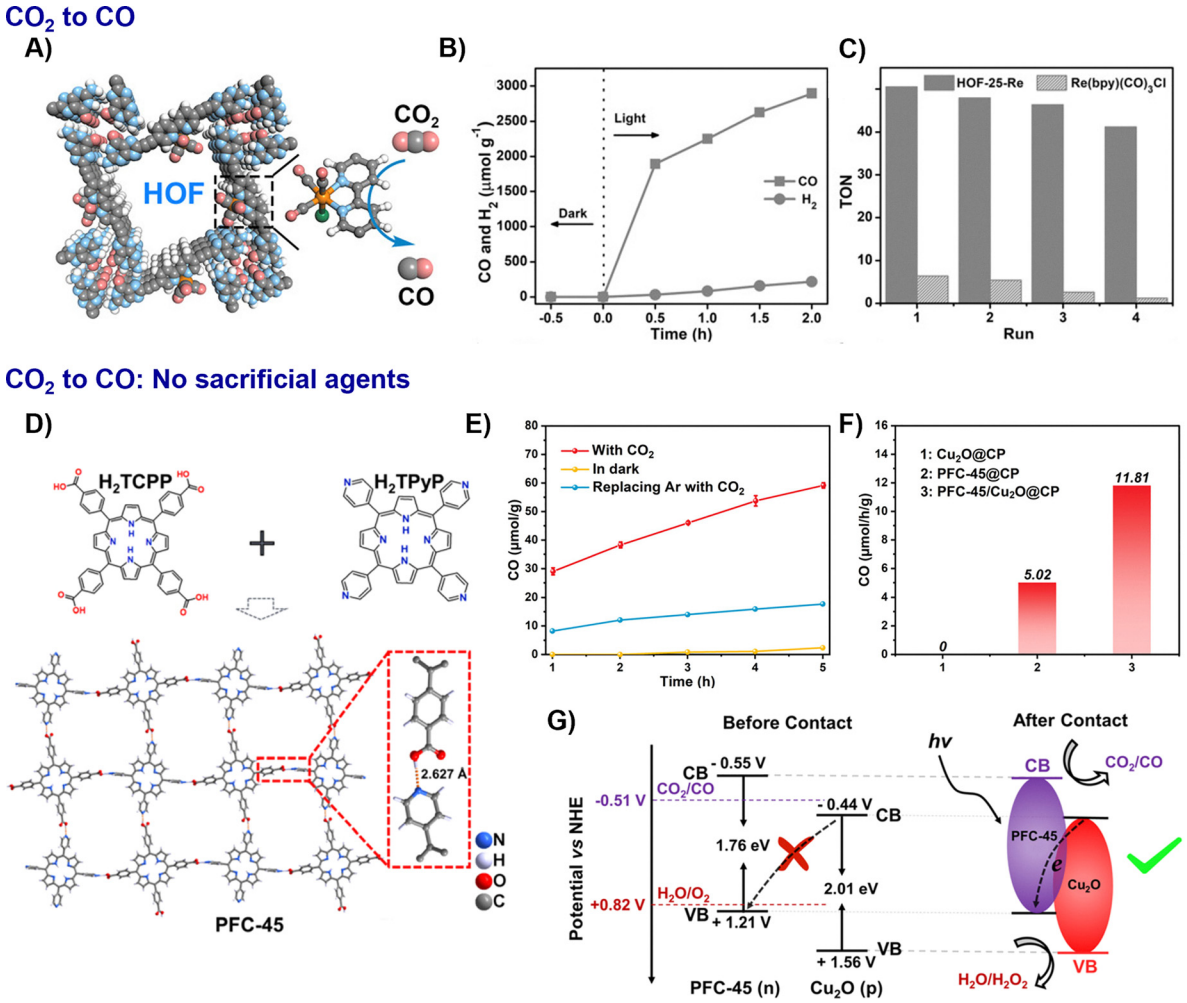

Fig. 10 Representative examples of nano-HOFs and its composites used in CO_2 conversion. HOF-25-Re:[81] (A) proposed structure, (B) time-dependent CO and H_2 evolution for the visible-light irradiated photocatalytic system, (C) the TON comparison of the CO_2 photoreduction between HOF-25-Re and Re(bpy)$(CO)_3$Cl, adapted with permission from ref. 81, Copyright 2021 Wiley-VCH; PFC-45/Cu_2O:[41] (D) structure of PFC-45; (E) control experiments of photocatalytic CO_2 reduction under visible-light irradiation over PFC-45/Cu_2O@CP, (F) CO production rate, (G) schematic diagram of charge transfer between p-type Cu_2O and n-type PFC-45, adapted with permission from ref. 41, Copyright 2022 ACS.

functional enzymes into cells with over 90% efficiency *via* clathrin-independent endocytosis. The encapsulated CAT (CAT@TA-HOFs) effectively reduced reactive oxygen species (ROS) in neuroblastoma cells under oxidative stress, improving cell viability from 35% to 60% and demonstrating the therapeutic potential of HOF-based enzyme delivery systems for neuroprotection.[69]

A breakthrough was achieved by using mesoporous HOFs simultaneously featuring small particle sizes (<100 nm) and large mesopores (>2 nm) to encapsulate enzymes. This design, exemplified by TaTb, effectively overcomes the mass transfer limitations of earlier carriers. When immobilising lactate dehydrogenase (LDH), the composite LDH@TaTb achieved a catalytic efficiency (K_{cat}/K_m) approaching 99.7% of the free enzyme, a significant enhancement over ZIF-8 and BioHOF-1 benchmarks.[68] Chen and Ouyang *et al.* found that HOF encapsulation can precisely manipulate enzyme function as well. Encapsulating cytochrome *c* (Cyt *c*) in HOF-101 induced a conformational switch from a native hexa-coordinated state to a non-native, catalase-like penta-coordinated state (Fig. 12D and E). This Cyt *c*@HOF-101 composite showed improved H_2O_2 decomposition activity, a functionality not present in the native enzyme and not achievable with MOF encapsulants, showcasing the unique ability of HOF scaffolds to confer novel catalytic properties.[83]

Recent advances demonstrate the power of protein-integrated HOFs in enabling sophisticated biorthogonal catalysis for targeted therapy. One strategy employs mitochondria-targeted HOFs (RuB-HOFs) that function as light-triggered photocatalysts. Co-encapsulation of CAT creates a dual-action platform for concurrent H_2S release and reactive oxygen species scavenging, offering neuroprotection.[84] To address the challenge of metabolic inactivation, a subsequent study designed a ferric porphyrin-based HOF that is intracellularly activated by glutathione. This platform simultaneously releases the anticancer drug 5-fluorouracil (5FU) and its inhibitor,

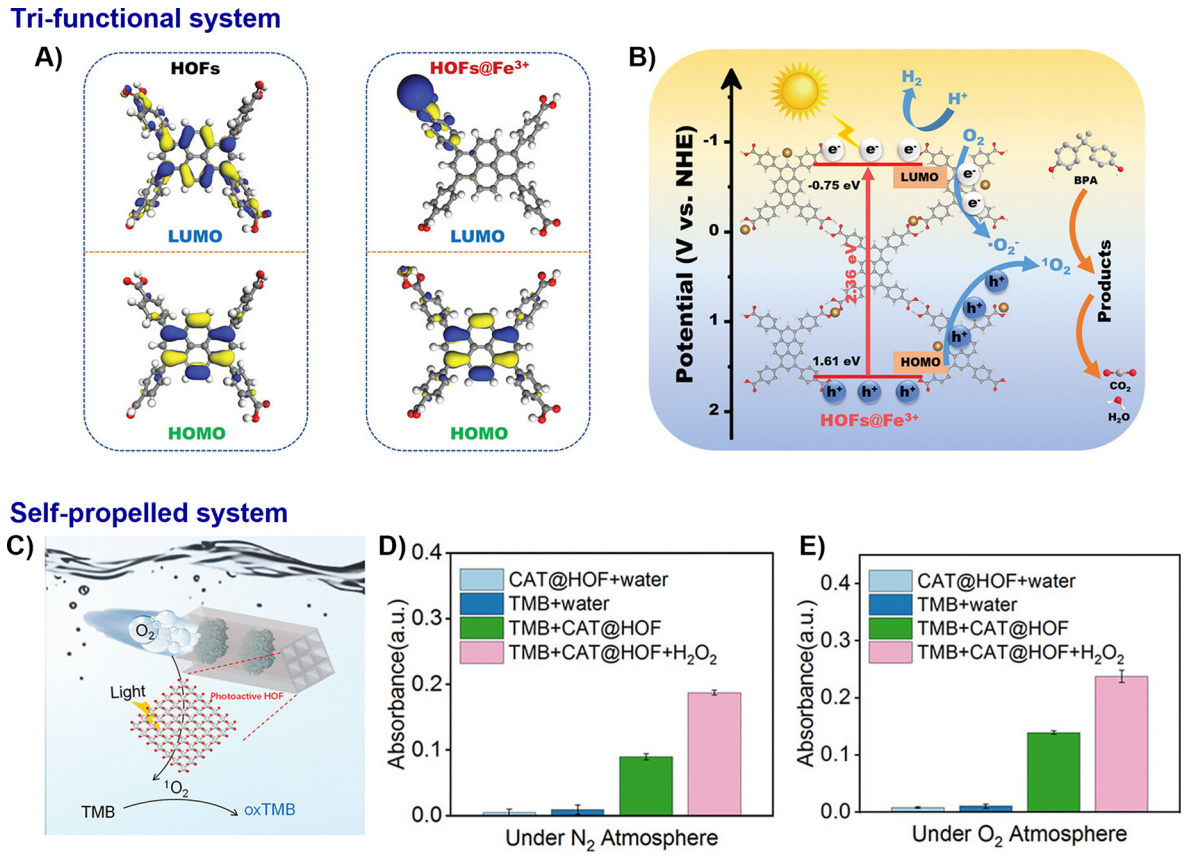

Fig. 11 Representative examples of nano-HOFs and its composites used in environmental catalysis. HOF@Fe^{3+}:[82] (A) LUMO and HOMO orbitals distribution in HOFs and HOFs@Fe^{3+} from DFT calculation, (B) photocatalytic mechanism of HOFs@Fe^{3+}, adapted with permission from ref. 82, Copyright 2023 Wiley-VCH; CAT@; HOF:[67] (C) schematic presentation of the photocatalytic oxidation of TMB using CAT@HOF, (D) the enhancement of photocatalysis by self-propelling CAT@HOF under N_2 atmosphere, (E) under O_2 atmosphere, adapted with permission from ref. 67, Copyright 2023 Wiley-VCH.

5-ethynyluracil (5EU), which protects the drug from degradation. This approach of co-releasing a drug and its protector enhanced therapeutic efficacy in the metastatic tumour model tested (Fig. 12F–H).[85]

Other catalytic systems. Beyond the above reactions, HOF nanocomposites continue to expand into new catalytic domains. For example, the HOF-102/cotton composite achieves 100% conversion of a mustard gas simulant (2-chloroethyl ethyl sulfide, CEES) to the non-toxic sulfoxide (2-chloroethyl ethyl sulfoxide, CEESO) within 30 minutes, with performance matching the pure HOF powder.[75] Wang *et al.* used H-bonding to assemble zero-dimensional CNQDs into 2D films. This unique architecture provided numerous H-bonding sites that dramatically enhanced the nitrogen reduction reaction (NRR) by facilitating N_2 fixation, achieving a high ammonia (NH_3) yield rate of 75.07 μg h^{-1} mg^{-1}.[32]

4.3. Energy storage

HOFs and its composites have shown the ability to address key challenges across diverse electrochemical platforms, ranging from battery electrodes to ion-conducting membranes, highlighting their significant potential as a unifying materials platform for energy technologies.

Metal-ion battery. In the realm of metal-ion batteries, HOFs have demonstrated exceptional performance as both cathodes and anodes. As cathodes for Li-ion batteries, frameworks like G_2PDI exhibit high operating voltages (~1.9–2.3 V *vs.* Li^+/Li), notable capacity retention (>93% after 300 cycles), and excellent Coulombic efficiency (>99.6%), mainly attributed to its stable porous structures and efficient electron and ion transport pathways.[29] Chen and Zhang *et al.* further applied HOF-FJU-1 in the fabrication of Li–CO_2 batteries (Fig. 13A and B). Its robust framework, featuring periodically aligned cyano groups, serves a triple function: inducing the homogeneous deposition of Li_2CO_3 to accommodate volumetric change, anchoring uniform Ru NPs to create highly efficient sites for CO_2 reduction/evolution, and providing ordered open channels for rapid gas and ion transport. This synergistic design enables Li–CO_2 batteries to achieve stability over 1800 hours and maintain a low overpotential of 1.96 V even at a high current density of 5 A g^{-1}.[60]

In addition to Li^+ batteries, the robust, multi-site H-bonding in frameworks like HOF-DAT was evaluated as a cathode

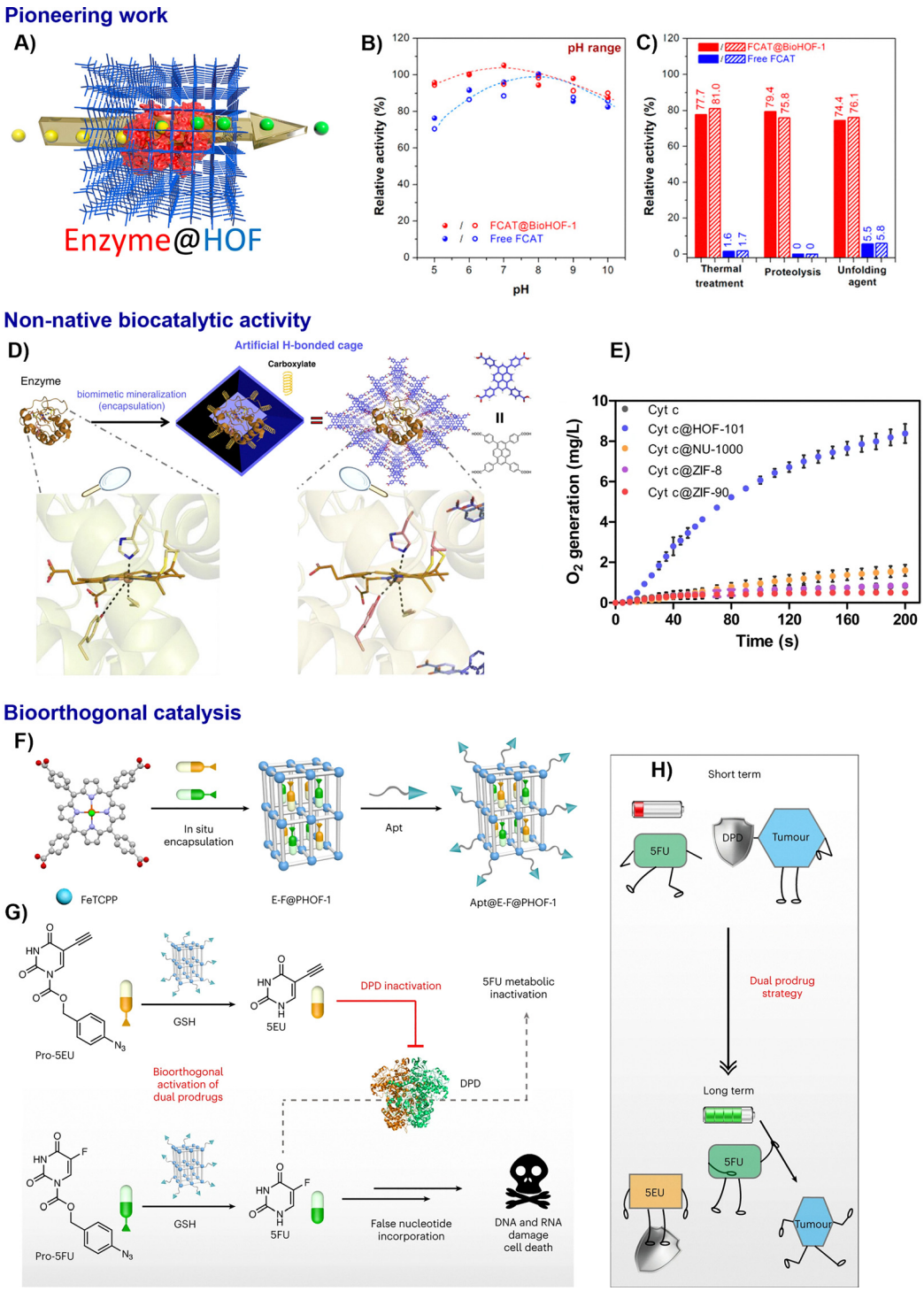

Fig. 12 Representative examples of nano-HOFs and its composites used in biocatalysis. BioHOF-1:[15] (A) schematic presentation of the enzyme encapsulation in HOFs, (B) relative activity of free FCAT and FCAT@BioHOF-1 at different Ph, (C) relative activity (%) of free FCAT and FCAT@BioHOF-1 after various treatment, adapted with permission from ref. 15, Copyright 2020 ACS; Non-native biocatalytic activity:[83] (D) schematic illustration of the designed H-bonded nanocage for modulating the conformation of an enzyme, Cyt *c* (PDB: 6k9i), (E) CAT-like bioactivities, adapted with permission from ref. 83, Copyright 2022 Springer Nature; HOF-based biorthogonal prodrug activation for chemotherapy:[85] (F) illustration of the synthesis of Apt@E-F@PHOF-1, (G) the chemotherapy mechanism of Apt@E-F@PHOF-1, (H) diagram of the dual drug strategy. Apt, aptamer AS1411; F, pro-5FU; E, pro-5EU, adapted with permission from ref. 85, Copyright 2023 Springer Nature.

material for Na-batteries. It delivered a high reversible capacity of 144 mAh g^{-1} at 50 mA g^{-1}, excellent rate capability (109 mAh g^{-1} at 2 A g^{-1}), and good cycling stability, retaining 73 mAh g^{-1} after 10 000 cycles at 1 A g^{-1}.[30] Subsequent studies

have built upon this by engineering HOFs with specific redox-active motifs. For instance, HOFs-8 utilizes its carbonyl (C═O) groups as the primary redox-active centres for Na^+ storage, while its flexible H-bonding network accommodates volume changes (Fig. 13C and D). This design delivered a high reversible capacity (172.9 mAh g^{-1}) and notable rate performance, while maintaining its capacity 107.9 mAh g^{-1} even at 10 °C.[36]

Compared to Na^+ and Li^+, K^+ has lower Lewis acidity, which benefits the enhancement of the migration rate and transference number for K^+ in liquid electrolytes.[86] Meng and Mai *et al.* fabricated an H-NDA-G cathode by *in situ* synthesis of H-NDA on GO, forming a 3D ''HOF-GO-HOF'' sandwich conductive network *via* hydrogen bonding and π–π interactions. The weak electronic coupling within this network establishes charge transfer channels and an interconnected conductive framework, promoting efficient K^+ redox reactions. As a result, the electrode achieved a high capacity of 120 mAh g^{-1} at 0.1 A g^{-1}.[50]

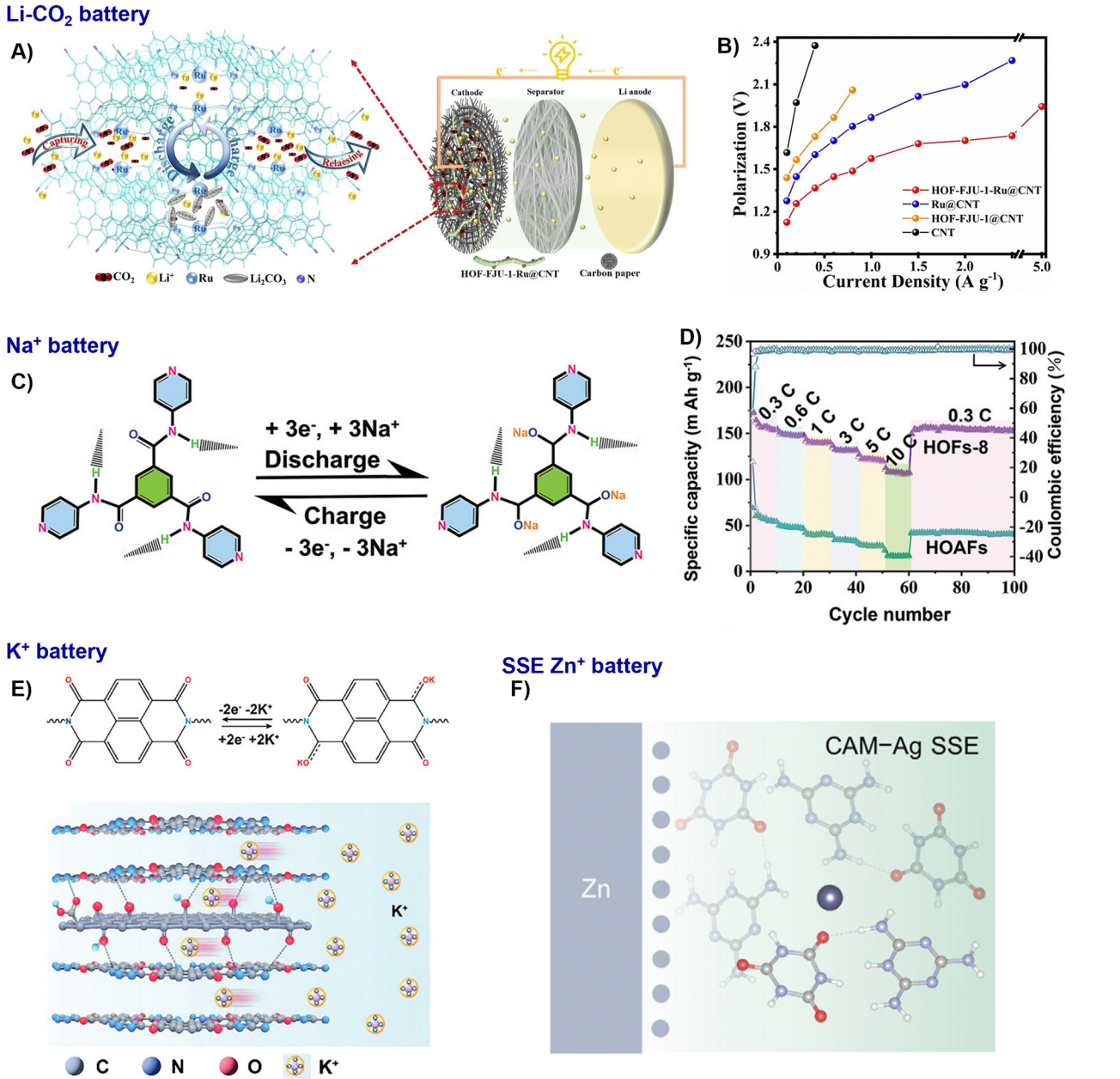

Fig. 13 Representative examples of nano-HOFs and its composites used in batteries. Li–CO_2 battery:[60] (A) schematic diagram of a Li–CO_2 battery, (B) battery overpotentials at various current densities, adapted with permission from ref. 60, Copyright 2023 Wiley-VCH; Na^+ battery:[30] (C) schematic illustration of the sodiation/desodiation process of the HOFs-8 electrode, (D) rate capabilities of HOFs-8 and HOAFs at different current rates from 0.3 to 10 C, adapted with permission from ref. 30, Copyright 2023 Wiley-VCH; K^+ battery:[86] (E) reaction mechanism of H-NDA-G and schematic representation of potassium storage in H-NDA-G based on interface decoupling, adapted with permission from ref. 86, Copyright 2024 Wiley-VCH; Zn^+ battery:[54] (F) schematic illustration of interface chemistry of Zn electrodes in CAM-Ag SSE. Adapted with permission from ref. 54, Copyright 2025 Wiley-VCH.

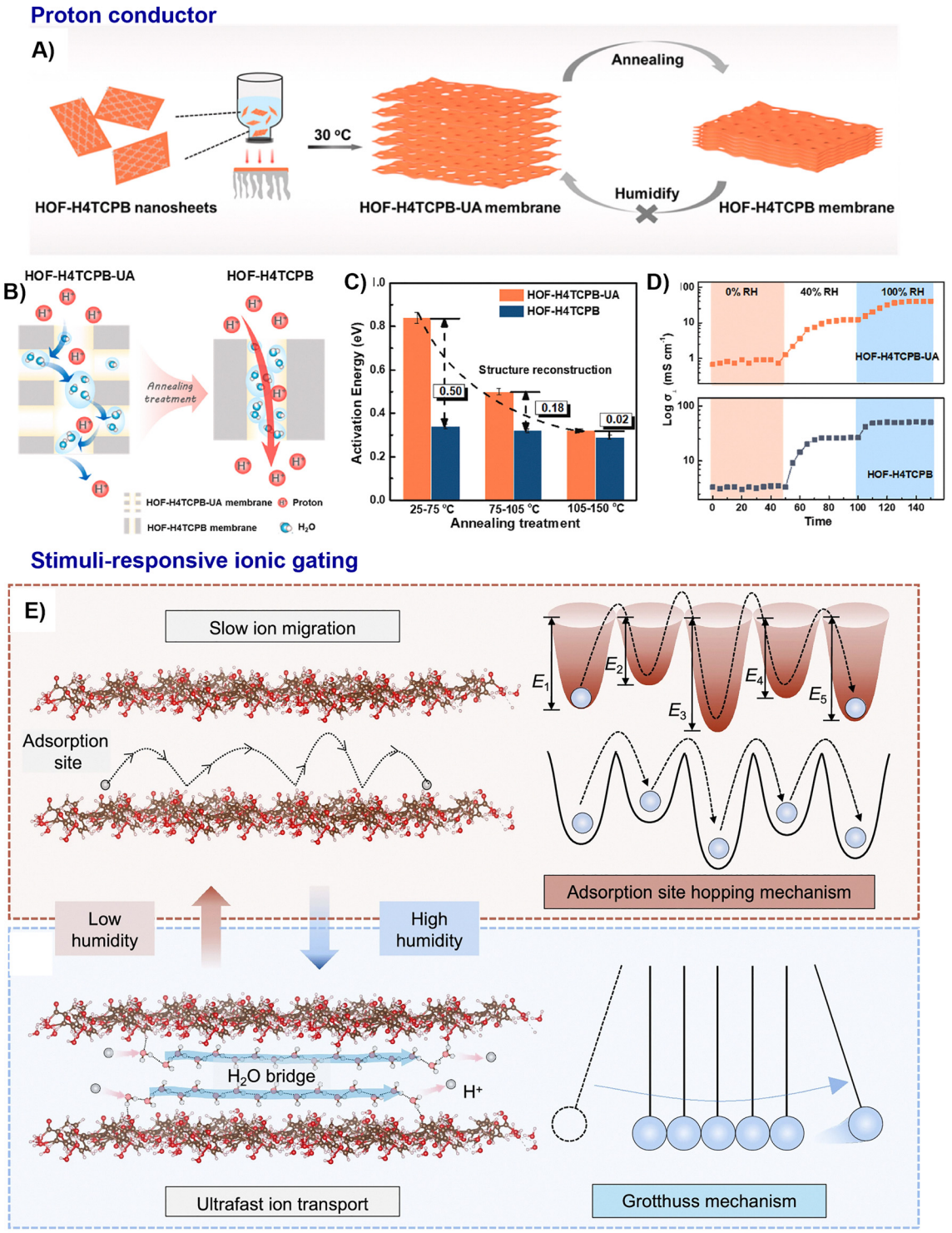

Fig. 14 Representative examples of nano-HOFs and its composites used in proton conductor. HOF-H4TCPB membrane:[44] (A) schematic preparation of HOF-H4TCPB membrane, (B) proton conduction in HOF-H4TCPB membrane at low humidity, (C) activation energy of HOF-H4TCPB membrane at various temperature range under 0% RH, (D) time-dependent vertical conductivity under different RH at 60 °C for 150 min, adapted with permission from ref. 44, Copyright 2022 Elsevier Inc, (E) the reversible formation and disruption of humidity-induced water bridges within HOFs facilitates the switching of proton transport mode from the adsorption site hopping of the Grotthuss mechanism, adapted with permission from ref. 74, Copyright 2025 Springer Nature.

Solid-state electrolytes (SSE) are safer and more stable in contrast to the conventional aqueous analogues. Xu and Wang *et al.* engineered a HOF-based solid-state electrolyte (CAM-Ag) for zinc-ion batteries by introducing Ag–N

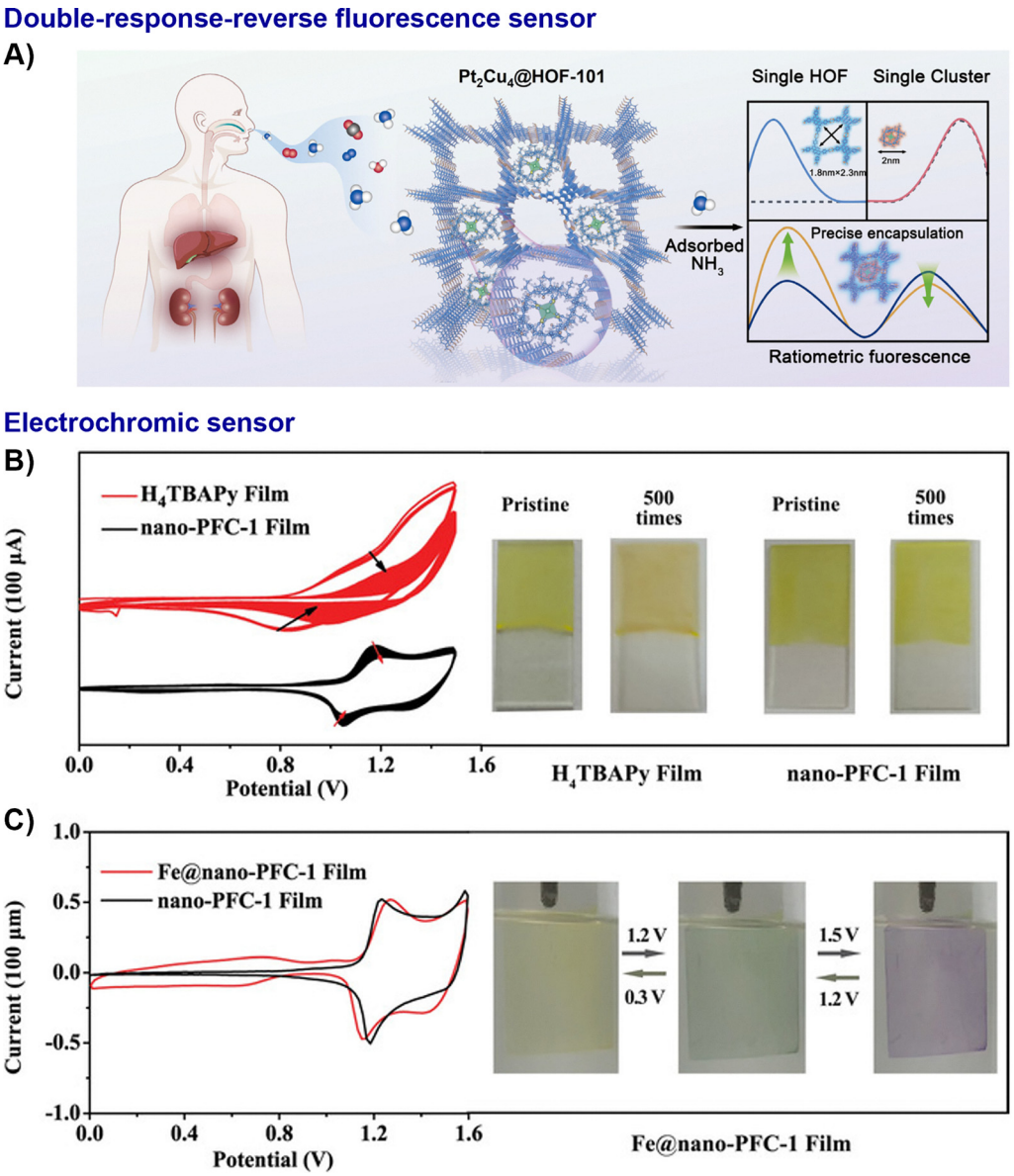

Fig. 15 Representative examples of nano-HOFs and its composites used in optical sensor. (A) Schematic illustration of the construction of Pt_2Cu_4@HOF-101 for double-response-reverse NH_3 fluorescence sensing,[59] adapted with permission from ref. 59, Copyright 2025 Elsevier Inc; nano-PFC-1 film:[40] (B) long-term CV scans (500 cycles) of the amorphous H_4TBAPy film andnano-PFC-1 film at a scan rate of 20 mV s^{-1} and corresponding photographs of films in the pristine state and after 500 CV cycles, (C) CV curves of the Fe@nano-PFC-1 and nano-PFC-1 films at a scan rate of 5 mV s^{-1} and photographs of the Fe@nano-PFC-1 film during CV cycles, adapted with permission from ref. 40, Copyright 2020 Wiley-VCH.

coordination bonds to induce a crystal transformation (Fig. 13F). This strategy created shortened Zn^{2+} conduction pathways, yielding a high ionic conductivity of 1.14×10^{-4} S cm^{-1} and an exceptional Zn^{2+} transference number of 0.72. The material's abundant H-bonding network effectively suppresses hydrogen evolution and by-product formation, while promoting uniform ion deposition to prevent dendrites.[54]

Proton conductor. Beyond batteries, HOFs can act as proton-conducting membranes, a critical component for fuel cells. Through strategic temperature-induced structural reconstruction, HOF membranes can be engineered to form compact architectures with continuous hydrogen-bond networks and biomimetic water channels (Fig. 14A–D). This design strategy yields notable proton conductivity (59.8 mS cm^{-1}), which rivals that of commercial Nafion—and enables efficient hydrogen fuel cell operation even under low relative humidity.[44]

A stimuli-responsive ionic gating behaviour was observed on HOF-H4TCPB nanosheet with a record proton gating ratio of 5740, allowing its conductivity to switch by orders of magnitude in response to humidity (Fig. 14E). This dramatic change is driven by a shift from a slow, high-energy hopping mechanism at low humidity (2.06 eV barrier) to an ultrafast Grotthuss mechanism at high humidity (0.33 eV barrier), facilitated by the formation of water bridges. This property was further successfully harnessed for real-world applications, including soil moisture monitoring and wireless respiratory rate tracking,

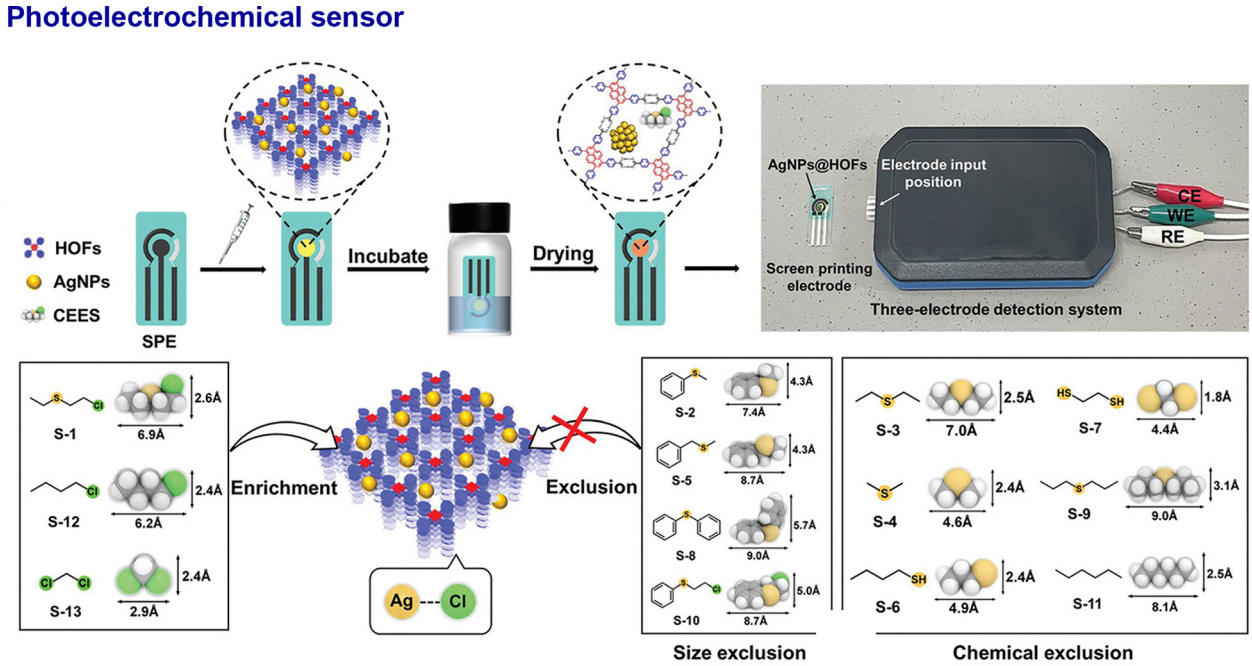

Fig. 16 Representative examples of nano-HOFs and its composites used in sensoring. AgNPs@HOF-101-10:[64] scheme for the fabrication of the CEES PEC sensor and molecular recognition steps to capture CEES, adapted with permission from ref. 64, Copyright 2022 Wiley-VCH.

showcasing a novel approach for non-contact physical sensing.[74]

4.4. Sensor

The structural and functional versatility of HOFs allows them to be tailored for a vast sensing landscape: from detecting specific chemical and biological analytes with high precision to monitoring physical environmental changes. To date, HOF-based nanocomposites have demonstrated great potential for use in various sensing platforms, including optical, electrochromic, electrochemical, photoelectrochemical, and biological sensors. Recently, an optical sensor was fabricated, where two kinds of NH_3 recognition sites, p-conjugated HOF and luminescent Pt_2Cu_4 nanocluster, were precisely assembled for ratiometric fluorescence sensing (Fig. 15A). The electron cloud interactions, enhanced by the nanoscopic quantum confinement effect of the metal clusters within the Pt_2Cu_4@HOF-101 composite, give rise to a distinctly different dual-fluorescence response signal toward NH_3. This unique response enables accurate quantification of NH_3 concentrations in the breath of liver and kidney disease patients, with a limit of detection (LOD) as low as 0.7 ppm. This combination of high sensitivity and selectivity demonstrates the potential of the system for non-invasive diagnosis through simple breath analysis.[59] Analogously, the intrinsic redox activity of pyrene units in the nano-PFC-1 film forms the basis of an electrochromic sensor, exhibiting a reversible behaviour, ideal for visual sensing applications. Moreover, a multi-state electrochromic behaviour enables successive colour changes from yellow to green to blue-violet by the introduction of additional Fe^{3+}/Fe^{2+} redox couples (Fig. 15B and C).[40] White and Foster *et al.* developed HOF-based nanosheets which, due to their high surface area and exposed active sites, achieved a high Rhodamine B quenching efficiency (93–95%) significantly higher than their bulk counterparts (<5%).[35] HOFs also provide an ideal matrix to enhance sensitivity in the realm of electrochemical and photoelectrochemical sensors. The plasmonic effect of AgNPs@HOF boosted the photocurrent, enabling a highly selective photoelectrochemical (PEC) sensor for CEES detection. This sensor achieved a LOD of 15.8 nmol L^{-1} with excellent discrimination against 13 potential interferents (Fig. 16). It is notable that AgNPs@HOF-101-10 achieved a photocurrent of 1.91 μA, over three times that of pristine HOF-101.[62] For chemiresistive sensing, exfoliated 2D L-HOF-199 nanosheets demonstrate high sensitivity towards NO_2 (152% to 5 ppm) and a low LOD of 15 ppb at room temperature. In contrast to the bulk crystals, the sensitivity and response speed were increased 3.25 times and more than twice, respectively.[87]

Furthermore, HOFs excel in biosensing. The large mesopores of MHOF-101 enable efficient multi-enzyme cascade reactions for detecting clinical biomarkers like glucose and uric acid in point-of-care biosensors.[72]

4.5. Chemo- and phototherapy

Chemotherapy relies on systemic pharmacological action, phototherapy enables localized light-mediated ablation, and chemo-phototherapy integrates both to achieve synergistic antitumor effects with reduced systemic toxicity. HOFs have recently emerged as promising candidates for photothermal therapy (PTT), photodynamic therapy (PDT) and chemo-photodynamic therapy (CPDT), owing to their tuneable photophysical properties, excellent biocompatibility, and versatile functionalization capabilities. Through rational structural design and composite engineering, researchers have developed

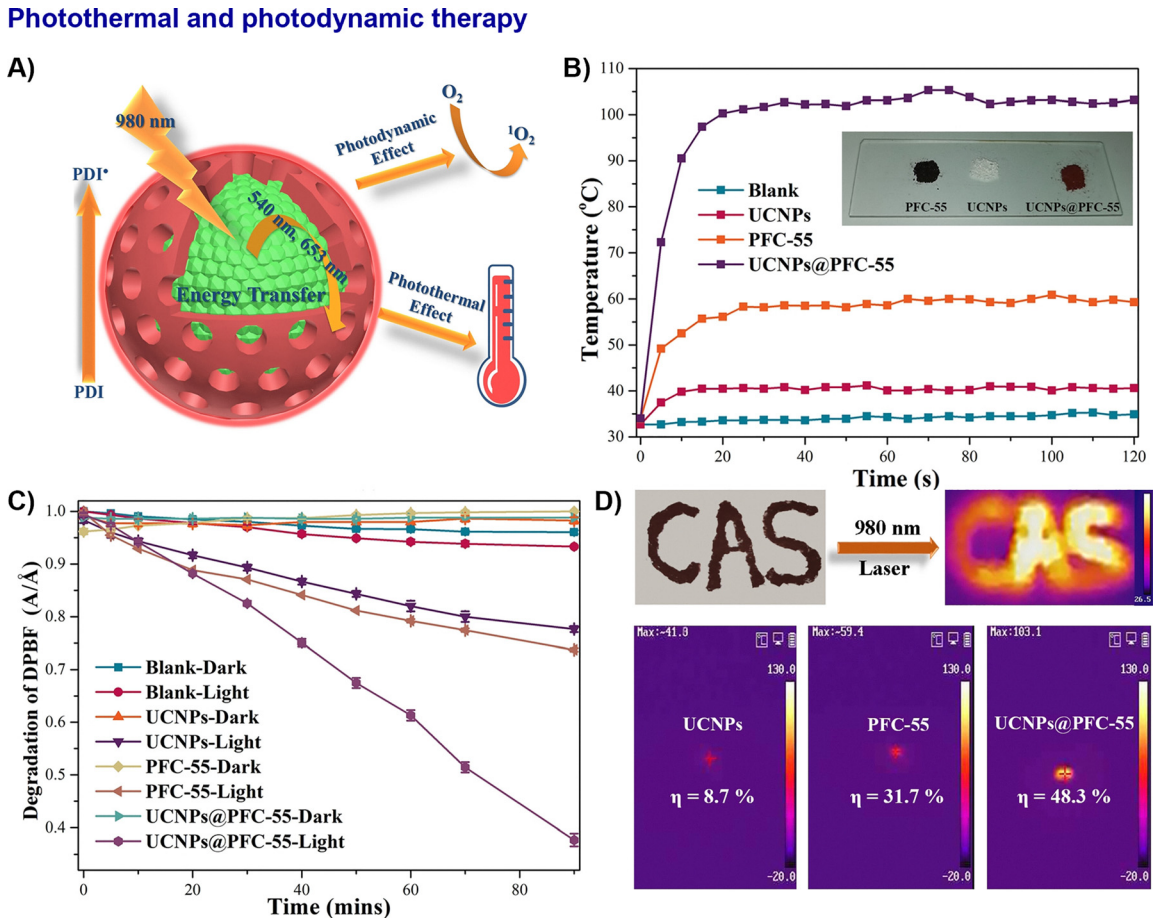

Fig. 17 Representative example of nano-HOFs and its composites used in photothermal therapy. UCNPs@PFC-5:[57] (A) RET process from UCNPs "core" to PFC-55 "shell" for achieving NIR-response photo-thermal and photodynamic effect, (B) photothermal conversion curves on quartzglass under NIR irradiation (980 nm, 1.5 W cm^{-2}), (C) time-dependent absorbance of DPBF solution at 413 nm, (D) IR camera images of patterned letter made of UCNPs@PFC-55, adapted with permission from ref. 57, Copyright 2021 Wiley-VCH.

a variety of high-performance HOF-based PTT and PDT agents that address key limitations of conventional materials, such as limited absorption range, low energy conversion efficiency, and shallow tissue penetration.

To overcome the inherent limitation of most HOFs absorbing primarily in the UV-visible range, core–shell composite strategies have been successfully developed. For instance, the integration of UCNPs with HOFs *via* luminescence resonance energy transfer (LRET) has enabled deep-tissue NIR activation.[57,58,88] A NIR-responsive photothermal and photodynamic synergistic platform, UCNPs@PFC-55, converts 808 nm NIR light to visible emissions, which then activate the HOF shell through LRET with 58.3% efficiency (Fig. 17A–D).[57]

HOFs can serve as versatile platforms for combination therapies. Early work by Liu and Cao *et al.* incorporated Doxo into photoactive Nano-PFC-1, enabling synergistic chemo-photodynamic therapy with reduced systemic toxicity.[89] Subsequent studies, such as the exfoliation of 3D HOFs into 1D nanoribbons, further increased drug loading capacity and allowed triple-modal chemo-photodynamic-photothermal therapy under dual-wavelength irradiation.[46] Enzyme-loaded systems like Ce6@EnHOF-101 have also been designed to execute synergistic photobiocatalytic cascades, modulating the tumour microenvironment for enhanced therapeutic outcomes.[65]

4.6. Other applications

Recent advances have underscored the potential of porous frameworks such as MOFs and HOFs in biomedical fields like drug delivery.[89] In particular, HOFs offer a unique advantage: the dynamic nature of their hydrogen bonds facilitates stimuli-responsive drug release. For example, Chen and Wang *et al.* recently introduced HOFs as programmable platforms for focused ultrasound (FUS)-triggered drug activation, enabling precise control over cellular events in deep brain tissue. By systematically modulating hydrogen-bond density and the number of aromatic fused rings within the organic ligands, the authors established a predictive model that correlates molecular architecture with ultrasound activation thresholds. This rational design facilitated 'sono-chemogenetics,' where FUS-triggered scission of supramolecular interactions prompted the instantaneous release of neuromodulators from

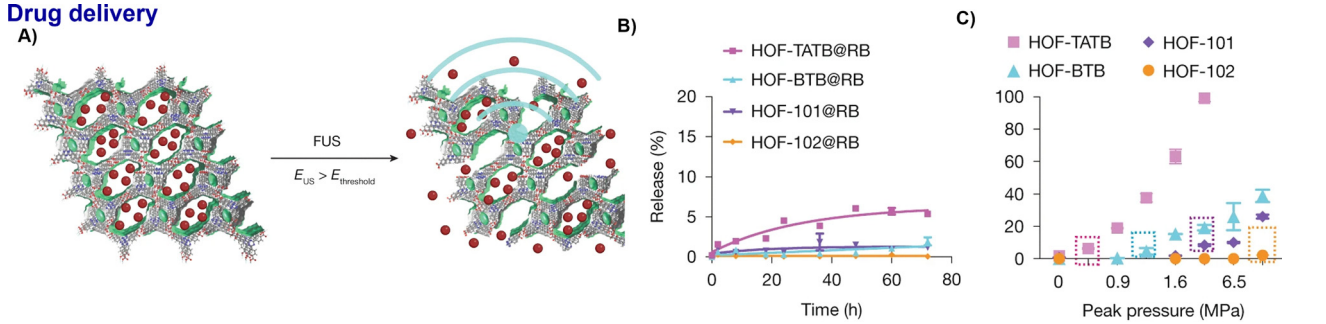

Fig. 18 HOFs as ultrasound-programmable delivery platform:[90] schematic of ultrasound-triggered drug release from HOF nanocrystals, with drug release occurring when $E_{US} > E_{threshold}$, (B) The free dye release from HOF nanocrystals without ultrasound stimulation, (C) ultrasound-triggered dye release from HOF nanocrystals after 90 s of stimulus, adapted with permission from ref. 90, Copyright 2025 Springer Nature.

HOF nanocrystals. This strategy achieves spatiotemporal control of deep neural circuits with second-level latency, offering a versatile, non-invasive paradigm for targeted molecular delivery. (Fig. 18A–C).[90]

Beyond drug delivery, antimicrobial activity was also explored in HOF composites. For example, HOF-101-F@PVDF-HFP nanofibers demonstrated good singlet oxygen ($^1O_2$) generation under green light (520 nm), achieving a 63 mmol g^{-1} of $^1O_2$ in 20 minutes—nearly twice that of pure HOF-101-F microcrystalline powder (using 0.5 wt% HOF-101-F@PVDF-HFP formulation). These nanofibers exhibited rapid, broad-spectrum antimicrobial activity, inactivating >94% of *Escherichia coli*, among others, within 5 minutes under ambient light.[33]

In addition to phototherapy, HOF-based composites have shown potential in other photothermal applications, such as water evaporation. A notable example is Ag@oxPFC-1, which exhibits a photothermal conversion efficiency of 69.8% under 808 nm laser irradiation due to efficient non-radiative decay. This composite also exhibited great promise as an interfacial solar evaporator, which exhibited a water evaporation rate of 1.445 kg m^{-2} h^{-1} with 93.6% efficiency (Table 1).[63]

5. Conclusions and perspective

In sum, this review has systematically outlined the methodologies for transforming bulk HOFs into nanostructured materials and nanocomposites. The transition to the nanoscale proves pivotal in terms of properties and versatility, enabling enhancements in pore accessibility, stability, and electronic conductivity that collectively improve active site accessibility, mass transport efficiency, and charge separation capability. These functional improvements establish HOF nanomaterials as promising platforms for advanced applications, including catalysis, energy storage, separations, and chemo- and phototherapy. Despite these advances, the rational design and practical of HOF nanomaterials remain constrained by several fundamental challenges, which also define key avenues for future research. Structural predictability: one major bottleneck lies in predictive materials design. Unlike reticular frameworks such as MOFs and COFs, where strong coordination or covalent bonds enable relatively reliable structure prediction, the dynamic and reversible nature of hydrogen bonding in HOFs fundamentally complicates the *a priori* design of stable and functional architectures. Subtle changes in assembly conditions can lead to divergent polymorphic outcomes, undermining rational design efforts. Recent progress in crystal structure prediction and high-throughput computational screening has demonstrated considerable promise in establishing energy–structure–function relationships. However, the accuracy of these predictions remains highly dependent on the quality of force fields and the completeness of conformational sampling, particularly for large, flexible building blocks. Experimental validation therefore remains essential to ground computational predictions in physical reality. Stability *vs.* processability: a fundamental dilemma: strategies enhancing framework robustness (interpenetration, crosslinking) often reduce solution processability, while high processability typically yields insufficient stability for practical applications. Although some HOFs exhibit high stability under specific conditions, this often comes at the cost of the very processability that distinguishes HOFs from other porous materials. HOFs with stimuli-responsive assembly/disassembly for processing might offer a promising direction to decouple these competing demands. Additionally, how to harness the benefits of HOF flexibility should be explored in the future. Defects and disorders: defects and disorder are intrinsic to the soft and dynamic nature of HOFs, yet their role in functionality remains underexplored and poorly understood. On one hand, disorder may disrupt long-range pore regularity, compromising size-exclusion selectivity and structural integrity. On the other hand, localized defects could introduce additional binding sites, facilitate charge separation, or create reactive centres for catalysis. This dual role presents both a challenge and an opportunity. A systematic characterization and theoretical modelling are urgently needed to correlate defect structures with functional outcomes. Reproducibility and scale-up: the sensitivity of supramolecular assembly to subtle environmental variations (*e.g.* solvents purity, ambient humidity, temperature), can lead to significant batch-to-batch variability in crystallinity and porosity. This reproducibility issue is critical for practical applications yet frequently overlooked in laboratory studies. Besides, developing continuous

Table 1 Summary of nano-HOFs and their based nanomaterials

Name	Composites		Preparation	Application	Ref.
	HOFs	Composite			
Separation					
HOF-30@PI	HOF-30	Polyimide polymer	Solution-casting	H_2/CH_4 separation	*J. Membr. Sci.*, 2022, **643**, 120021
UPC-HOF-6	UPC-HOF-6	Al_2O_3	Solution-casting	H_2/N_2 separation	*Angew. Chem. Int. Ed.*, 2020, **59**, 3840
CB6-1	CB6-1	—	Solvothermal	SO_2/CO_2	*J. Mater. Chem. A*, 2020, **8**, 19799
HOF-BTB@AAO	HOF-BTB	Al_2O_3	Solution-casting	C_3H_6/C_3H_8 separation	*Nat. Commun.*, 2024, **15**, 634
PG-HOFs	PFC-1	NH_2-IL + bis-C_2 OH-IL + bis-C_2 Olefin + bis-C_2	Post-synthesis	Radioactive anions adsorption (I^-, IO_3^-, ReO_4^-)	*Sci. China Chem.*, 2024, **67**, 2958
HOF-TFN-2	PFC-1	PIP + PES + TMC	Post-synthesis	Dye separation	*Nanoscale Adv.*, 2021, **3**, 3441
^{CSMCRI}HOF2-P	^{CSMCRI}HOF2-P	—	Solvothermal	Uranium extraction	*Small*, 2024, **20**, 2306824
TFCHs	^{CSMCRI}HOF-1	—	Solvothermal	Uranium extraction	*Chem*, 2022, **8**, 2749
DFA-TPY	TPY	DFA	Solvothermal	Oils, microplastics capture	*Angew. Chem. Int. Ed.*, 2024, **63**, e202404452
Energy storage					
CAM-Ag	CAM	$AgNO_3$	Solvothermal + freeze-drying	Zn^{2+} battery	*Adv. Mater.*, 2025, **37**, 2500721
HOF-FJU-1-Ru@CNT	HOF-FJU-1	Ru@CNT	Solvothermal	CRR/CER/Li–CO_2 battery	*Angew. Chem. Int. Ed.*, 2023, **135**, e202311480
HOFs-8	HOFs-8	Acetylene black/cellulose sodium	Solvothermal	Na^+ battery	*Adv. Funct. Mater.*, 2024, **34**, 2314851
H-NDA-G	H-NDA	Graphene oxide	Solvothermal	K^+ battery	*Adv. Funct. Mater.*, 2025, **35**, 2407452
HOF-DAT	HOF-DAT	—	*In situ* synthesis and assembly	Na^+ battery	*Adv. Mater.*, 2021, **33**, 2106079
G_2PDI	G_2PDI	PVDF + CB	Solution-casting	Li^+ battery	*Nat. Chem.*, 2017, **9**, 466
HOF-H4TCPB	HOF-H4TCPB	—	Solvothermal	Proton conductor/hydrogen fuel cell	*J. Membr. Sci.*, 2022, **664**, 121118
HOF-H4TCPB/BC	HOF-H4TCPB	Bacterial cellulose	Solvothermal	Proton gating/soil moisture monitor	*Nat. Commun.*, 2025, **16**, 754
Catalysis					
TiO_2@HOF-TCPB-373	HOF-TCPB-373	TiO_2	Milling/sonication	Photo-degradation	*Appl. Surf. Sci.*, 2024, **644**, 158770
PFC-1/CNNS	PFC-1	CNNS	Solvothermal	HER/photo-degradation	*J. Photochem. Photobiol., A*, 2023, **435**, 114292
LDH@TaTb	TaTb	LDH(E)	Solvothermal	Biocatalysis	*Chem. Eng. J.*, 2023, **468**, 143609
Cyt c@HBF-1	PFC-1	Cyt-*c*	Solvothermal	Biocatalysis	*Chem*, 2021, **7**, 2722
Cyt c@HBF-2	HBF-2				
HOFs@M^{n+}	PFC-1	Fe^{3+}, Cu^{2+}, Zn^{2+}	Solvothermal	Photo-degradation/HER	*Adv. Funct. Mater.*, 2023, **33**, 2300954
MHOF-101	PFC-1	β-Gal-GOx-HRP GOx-HRP	Solvothermal	Biosensors/biocatalysis	*Angew. Chem. Int. Ed.*, 2021, **60**, 23608
HOF-25-Re	HOF-25	$Re(CO)_5Cl$	Solvothermal	CO_2 reduction	*Angew. Chem. Int. Ed.*, 2021, **60**, 8983
HOF-25-Ni@GO	HOF-25	GO, $Ni(ClO_4)_2{\cdot}6H_2O$	Sonication+ solvothermal	CO_2 reduction	*Angew. Chem. Int. Ed.*, 2022, **61**, e202211482
CAT@RuB-HOFs	RuB-HOFs	CAT	Solvothermal	Biocatalysis	*Angew. Chem. Int. Ed.*, 2023, **62**, e202312784
HOF/COF	PFC-1	Py-COF	Solvothermal	HER	*Angew. Chem. Int. Ed.*, 2025, **64**, e202414229
MTC@$Co_{1-x}Fe_xS_2$	MTC	$Fe(NO_3)_3$, $C_o(NO_3)_2$, thiourea	Solvothermal	OER	*Sustainable Energy Fuels*, 2024, **8**, 3174
M.CA	MA + CA	—	Solvothermal	HER	*ACS Omega*, 2022, **7**, 22440
M.TC	MA + TC				
B.TC	BP + TC				
HOF-19 ⊃ Pd(II)	HOF-19	Pd^{2+}	Solvothermal	Organic catalysis	*J. Am. Chem. Soc.*, 2019, **141**, 8737
protein@TA-HOFs	TA-HOFs	GFP/HRP/CAT/β-Gal	Solvothermal	Biocatalysis	*Angew. Chem. Int. Ed.*, 2021, **60**, 22315
FAOx@BioHOF-1	BioHOF-1	FAOx	Solvothermal	Biocatalysis	*J. Am. Chem. Soc.*, 2019, **141**, 14298

Table 1 (*continued*)

Name	Composites		Preparation	Application	Ref.
	HOFs	Composite			
FCAT@ BioHOF-1		FCAT			
HOF-102/cotton	HOF-102	Cotton	Solution-casting	Photocatalysis	*Cell Rep. Phys. Sci.*, 2020, **1**, 100024
PFC-45/Cu_2O@CP	PFC-45	Cu_2O@CP	Sonication/electrophoretic deposition	CO_2 reduction	*ACS Appl. Mater. Interfaces*, 2022, **14**, 21050
Cyt c@HOF-101	PFC-1	Cyt *c*	Solvothermal	Biocatalysis	*Nat. Commun.*, 2022, **13**, 4816
CNP	CNP	Pt	Solvothermal	HER/H_2O_2 evolution	*Nat. Nanotechnol.*, 2023, **18**, 307
H–S/TBAP-α	PFC-1	[FeFe]-hydrogenases	Solvothermal	HER	*ACS Catal.*, 2024, **14**, 18603
CAT@HOF	PFC-1	CAT	Solvothermal	OER	*Small Struct.*, 2023, **4**, 2200346
CNQD	MA + CA	—	Solvothermal	NRR/OER Zn–N_2 battery	*ACS Nano*, 2022, **16**, 9049
HOF-H_4TBAPy	PFC-1	Pt	Solvothermal	HER	*Nat. Catal.*, 2023, **6**, 574
Sensing					
HON-1	HON-1	—	Sonication	Fluorescence sensor	*Chem. Sci.*, 2021, **12**, 3322
HON-2	HON-2				
Pt_2Cu_4@HOF-101	PFC-1	Pt_2Cu_4	Solvothermal	Fluorescence sensor	*Chem*, 2025, **11**, 102457
L-HOF-199	L-HOF-199	—	Sonication	Chemiresistive NO_2 sensor	*Inorg. Chem.*, 2025, **64**, 1258
AgNPs@HOFs	PFC-1	AgNPs	Solvothermal + photo-reduction	Photoelectrochemical sensor	*Adv. Mater.*, 2022, **34**, 2202287
	HOF-102				
nano-PFC-1	PFC-1	FTO	Electrophoretic deposition	Electrochromic sensor	*Angew. Chem. Int. Ed.*, 2020, **59**, 22392
Chemo-phototherapy					
CSS@P-P	PFC-55	CSS + PAA	Solvothermal post-grafting	Cancer therapy	*Nano Today*, 2023, **48**, 101751
UCNPs@PFC-55	PFC-55	β-NaYF4:Yb,Er	Solvothermal+ post-synthesis	Bacterial inhibition	*Angew. Chem. Int. Ed.*, 2021, **60**, 25701
UCNPs@PFC-73-Ni	PFC-73-Ni	UCNPs	Solvothermal	Antimicrobial therapy	*Aggregate*, 2024, **5**, e481
HOF-101-H@PVDF-HFP	PFC-1	PVDF-HFP	Electrospinning	Antimicrobial	*Adv. Funct. Mater.*, 2023, **33**, 2214388
HOF-101-F@PVDF-HFP	HOF-101-F				
Doxo@Nano-PFC-1	PFC-1	Doxorubicin	Solvothermal	Chemo-photodynamic therapy	*Angew. Chem. Int. Ed.*, 2018, **57**, 7691
TCPP-1,3-DPP	TCPP-1,3-DPP	Doxorubicin	Sonication	Drug delivery/chemo and phototherapy	*ACS Appl. Nano Mater.*, 2019, **2**, 2437
MB@JZS-1	JZS-1	Methylene blue	Solvothermal	Antimicrobial	*ACS Appl. Mater. Interfaces*, 2022, **14**, 49875
Ce6@EnHOF-101	PFC-1	GOx + CAT + Ce6	Solvothermal	Bacterial inhibition/wound therapy	*JACS Au*, 2022, **2**, 2048
Apt@E-F@PHOF-1	PHOF-1	Apt + pro-5FU+ pro-5EU	Solvothermal	Cancer therapy	*Nat. Catal.*, 2023, **6**, 729
Other applications					
HOF-TATB	HOF-TATB	Clozapine N-oxide	Solvothermal	Drug delivery/deep-brain neuromodulation	*Nature*, 2025, **638**, 401
Ag@oxPFC-1	PFC-1	$AgNO_3$	Post-synthesis	Solar-driven water evaporator	*Sci. China Chem.*, 2025, **68**, 1
	HOF-14				

manufacturing approaches, such as flow chemistry, is needed for expanding to the large-scale practical use, since conventional batch synthesis methods (*e.g.*, slow solvent evaporation) are inherently unscalable. Conductivity: most HOFs are electrical insulators due to limited π–π conjugation. This intrinsic limitation can be overcome through the rational design of conductive or redox-active building blocks—such as π-conjugated systems, heteroatoms, or metal centres—or through composite formation with conductive supports like carbon nanotubes and graphene oxide. The convergence of enhanced conductivity with solution-based processability positions HOF-based materials as promising candidates for flexible, wearable, and next-generation electronic devices. Nanoscale features *vs.* crystallinity: pursuing nanoscale morphologies to enhance kinetics often compromises crystallinity, while highly crystalline bulk HOFs suffer from slow diffusion. Therefore, an alternative strategy lies in engineering anisotropic interactions: strong bonding along one direction to maintain long-range order, and weak interactions in orthogonal directions to facilitate nanoscale processing. 1D or 2D HOFs might exemplify this concept, where the directional assembly preserves crystallinity while allowing isolation of nanoscale morphologies.

Addressing these interconnected challenges demands a shift from empirical optimization toward integrated design frameworks. First, computationally guided design must evolve to capture not only ideal structures but also the dynamic disorder and condition-dependent behaviours that govern real-world HOF performance. Second, autonomous synthesis and continuous manufacturing should be leveraged not only to accelerate the discovery of functional materials but also to enhance reproducibility and scalability. Third, interfacial engineering, particularly for the formation of stable HOF-based nanocomposites, is essential for expanding HOF applications into emerging fields such as wearable electronics. In this context, transducing dynamic structural changes in response to external stimuli into readable signals represents an attractive direction that leverages the distinguishing flexibility of HOFs. Finally, advanced characterization must bridge the gap between nanoscale features and bulk crystallinity. The convergence of these complementary strategies will be pivotal in realizing HOFs as a versatile and practically relevant class of functional nanomaterials.

Author contributions

This review was conceptualized and coordinated by Dr Antonio Fernandez-Mato. The literature search and data curation were performed by Dr Qiang Zhu. Both authors contributed to the manuscript preparation.

Conflicts of interest

The authors declare no conflict of interest.

Abbreviations

1D	One-dimensional
$^1O_2$	Singlet oxygen
2D	Two-dimensional
3D	Three-dimensional
3D-ED	Three-dimensional electron diffraction
5EU	5-Ethynyluracil
5FU	5-Fluorouracil
AAO	Anodic aluminum oxide
Apt	Aptamer as1411
AQY	Apparent quantum yield
BC	Bacterial cellulose
BET	Brunauer–emmett–teller
bis-C_2	3,3′-divinyl-1,1′-(1,2-ethanediyl)-diimidazolium dibromide
Boc	*Tert*-butyloxycarbonyl
BP	Bipyridine
BTC	Benzene-1,3,5-tricarboxylic acid
CA	Cyanuric acid
CAM	Cyanuric acid–melamine
CAT	Catalase
CB	Carbon black;
Ce6	Chlorin e6
CEES	2-Chloroethyl ethyl sulfide
CEESO	2-Chloroethyl ethyl sulfoxide
CER	CO_2 evolution reaction
CNDQs	Carbon nitride-based quantum dots
CNNS	Carbon nitride nanosheets
CNP	2,6-Bis(4-cyanophenyl)-4-(9-phenyl-9*H*-carbazol-3-yl)-pyridine-3,5-dicarbonitrile
CNT	Carbon nanotube
CP	Carbon paper
COFs	Covalent organic frameworks
CPDT	Chemo-photodynamic therapy
CRR	CO_2 reduction reaction
Cryo-EM	Cryo-electron microscopy
CSP	Crystal structure prediction
CSS	$NaYF_4$:Yb^{3+}/Er^{3+}@$NaYF_4$:Nd^{3+}@$NaYF_4$
Cyt *c*	Cytochrome *c*
DMF	*N*,*N*-dimethylformamide
Doxo	Doxorubicin
EPD	Electrophoretic deposition
FAOx	Fluorescein-tagged alcohol oxidase
FCAT	Fluorescein-tagged catalase
FRET	Förster resonance energy transfer
FTO	Fluorine-doped tin oxide
GFP	Green fluorescent protein
GO	Graphene oxide
GOx	Glucose oxidase
HBFs	H-bonded biohybrid frameworks
HER	Hydrogen evolution reaction
HRP	Horseradish peroxidase
HOFs	Hydrogen-bonded organic frameworks
HONs	2D H-bonded organic nanosheets
ISSA	*In situ* synthesis and assembly

LDH	Lactate dehydrogenase
LOD	A limit of detection
LRET	Luminescence resonance energy transfer
MA	Melamine
MB^+	Cationic methylene blue
MMM	Mixed-matrix membrane
MNCs	Metal nanoclusters
MOFs	Metal–organic frameworks
MTC	Melamine–trithiocyanurate
M_xO_y	Metal oxides
NDI	Naphthalene diimide
NH_3	Ammonia
NH_2-BDC	2-Aminoterephthalic acid
NH_2-IL	1-Aminoethyl-3-vinylimidazolium bromide hydrobromide
NIR	Near-infrared
NPs	Nanoparticles
NRR	Nitrogen reduction reaction
NRs	Nanorods
NSs	Nanosheets
NTCDA	1,4,5,8-Naphthalenetetracarboxylic dianhydride,
NTCDA	1,4,5,8-Naphthalenetetracarboxylic dianhydride
OER	Oxygen evolution reaction
OH-IL	1-(2-Hydroxyl-ethyl)-3-vinyl imidazolium bromide
olefin	4-Penten-1-ol
PA	Polyamide
PAA	Polyacrylic acid
PDA	*p*-Phenylenediamine
PDI	Perylene diimide
PDT	Photodynamic therapy
PES	Polyethersulfone
PI	Polyimide
PIP	Piperazine
PTT	Photothermal therapy
PVDF-HFP	Poly(vinylidene fluoride-*co*-hexafluoropropylene)
PVP	Polyvinylpyrrolidone
RET	Resonance energy transfer
ROS	Reactive oxygen species
SSE	Solid-state electrolytes
TC	Trithiocyanuric acid
TFA	Trifluoroacetic acid
TFCHs	Thin film covalent hybrids
TFN	Thin film nanocomposite
TMC	1,3,5-Benzenetricarbonyl trichloride
TPBTC	N1, N3, N5-tris(pyridine-4-yl)benzene-1,3,5-tricarboxamide
UCNPs	Upconversion nanoparticles
Uox-HRP	Urate oxidase xanthine

Data availability

No primary research results, software or code have been included and no new data were generated or analysed as part of this review.

Acknowledgements

This work was partially supported by the Beatriz Galindo program (grant BG24/00084) from the Spanish Ministry of Science, Innovation and Universities

References

1 K. Geng, T. He, R. Liu, S. Dalapati, K. T. Tan, Z. Li, S. Tao, Y. Gong, Q. Jiang and D. Jiang, *Chem. Rev.*, 2020, **120**, 8814–8933.
2 C. S. Diercks and O. M. Yaghi, *Science*, 2017, **355**, eaal1585.
3 H. Furukawa, K. E. Cordova, M. O'Keeffe and O. M. Yaghi, *Science*, 2013, **341**, 1230444.
4 A. M. Wright, M. T. Kapelewski, S. Marx, O. K. Farha and W. Morris, *Nat. Mater.*, 2025, **24**, 178–187.
5 D. J. Duchamp and R. E. Marsh, *Acta Crystallogr., Sect. B*, 1969, **25**, 5–19.
6 M. Simard, D. Su and J. D. Wuest, *J. Am. Chem. Soc.*, 1991, **113**, 4696–4698.
7 X. Wang, M. Simard and J. D. Wuest, *J. Am. Chem. Soc.*, 1994, **116**, 12119–12120.
8 Y. He, S. Xiang and B. Chen, *J. Am. Chem. Soc.*, 2011, **133**, 14570–14573.
9 Q. Zhu, J. Johal, D. E. Widdowson, Z. Pang, B. Li, C. M. Kane, V. Kurlin, G. M. Day, M. A. Little and A. I. Cooper, *J. Am. Chem. Soc.*, 2022, **144**, 9893–9901.
10 B. Burger, P. M. Maffettone, V. V. Gusev, C. M. Aitchison, Y. Bai, X. Wang, X. Li, B. M. Alston, B. Li, R. Clowes, N. Rankin, B. Harris, R. S. Sprick and A. I. Cooper, *Nature*, 2020, **583**, 237–241.
11 A. Pulido, L. Chen, T. Kaczorowski, D. Holden, M. A. Little, S. Y. Chong, B. J. Slater, D. P. McMahon, B. Bonillo, C. J. Stackhouse, A. Stephenson, C. M. Kane, R. Clowes, T. Hasell, A. I. Cooper and G. M. Day, *Nature*, 2017, **543**, 657–664.
12 M. Mastalerz and I. M. Oppel, *Angew. Chem., Int. Ed.*, 2012, **51**, 5252–5255.
13 H. Wang, B. Li, H. Wu, T. L. Hu, Z. Yao, W. Zhou, S. Xiang and B. Chen, *J. Am. Chem. Soc.*, 2015, **137**, 9963–9970.
14 Q. Yin, P. Zhao, R. Sa, G. Chen, J. Lü, T. Liu and R. Cao, *Angew. Chem., Int. Ed.*, 2018, **130**, 7817–7822.
15 W. Liang, F. Carraro, M. B. Solomon, S. G. Bell, H. Amenitsch, C. J. Sumby, N. G. White, P. Falcaro and C. J. Doonan, *J. Am. Chem. Soc.*, 2019, **141**, 14298–14305.
16 L. Li, X. Zhang, X. Lian, L. Zhang, Z. Zhang, X. Liu, T. He, B. Li, B. Chen and X. H. Bu, *Nat. Chem.*, 2025, **17**, 727–733.
17 H. Liaquat, M. Imran, Z. Saddique, S. Latif, K. M. Al-Ahmary, A. Sohail, H. Raza and M. Ahmed, *J. Mol. Struct.*, 2025, **1320**, 140221.
18 X. Liu, G. Liu, T. Fu, K. Ding, J. Guo, Z. Wang, W. Xia and H. Shangguan, *Adv. Sci.*, 2024, **11**, 2400101.
19 B. Wang, R.-B. Lin, Z. Zhang, S. Xiang and B. Chen, *J. Am. Chem. Soc.*, 2020, **142**, 14399–14416.
20 R.-B. Lin, Y. He, P. Li, H. Wang, W. Zhou and B. Chen, *Chem. Soc. Rev.*, 2019, **48**, 1362–1389.

21 A. C. Grimsdale and K. Müllen, *Angew. Chem., Int. Ed.*, 2005, **44**, 5592–5629.
22 C. Ma, L. Qin, T. Zhou and J. Zhang, *Energy Environ. Sci.*, 2024, **17**, 8992–9026.
23 P. Soleimani Abhari, S. Gholizadeh, F. Rouhani, Y. L. Li, A. Morsali and T. F. Liu, *Inorg. Chem. Front.*, 2023, **10**, 6134–6159.
24 C. Chen, L. Shen, H. Lin, D. Zhao, B. Li and B. Chen, *Chem. Soc. Rev.*, 2024, **53**, 2738–2760.
25 Y. Zhang, M. Tian, Z. Majeed, Y. Xie, K. Zheng, Z. Luo, C. Li and C. Zhao, *Separations*, 2023, **10**, 196.
26 D. Yu, H. Zhang, J. Ren and X. Qu, *Chem. Soc. Rev.*, 2023, **52**, 7504–7523.
27 C. Halliwell, J. F. Soria and A. Fernandez, *Angew. Chem., Int. Ed.*, 2023, **62**, e202217729.
28 Y. Guo, C. Wang, G. Mo, Y. Wang, X. Song and P. Li, *Cryst. Growth Des.*, 2023, **23**, 7635–7646.
29 Y. L. Wu, N. E. Horwitz, K. S. Chen, D. A. Gomez-Gualdron, N. S. Luu, L. Ma, T. C. Wang, M. C. Hersam, J. T. Hupp, O. K. Farha, R. Q. Snurr and M. R. Wasielewski, *Nat. Chem.*, 2017, **9**, 466–472.
30 Y. Wu, X. Mao, M. Zhang, X. Zhao, R. Xue, S. Di, W. Huang, L. Wang, Y. Li and Y. Li, *Adv. Mater.*, 2021, **33**, 2106079.
31 J. Liang, S. Xing, P. Brandt, A. Nuhnen, C. Schlüsener, Y. Sun and C. Janiak, *J. Mater. Chem. A*, 2020, **8**, 19799–19804.
32 F. Wang, Q. Wang, S. Wang, K. Zhang, S. Jia, J. Chen and X. Wang, *ACS Nano*, 2022, **16**, 9049–9061.
33 Y. Wang, R. Cao, C. Wang, X. Song, R. Wang, J. Liu, M. Zhang, J. Huang, T. You, Y. Zhang, D. Yan, W. Han, L. Yan, J. Xiao and P. Li, *Adv. Funct. Mater.*, 2023, **33**, 2214388.
34 Z. X. Cai, Y. Xia, Y. Ito, M. Ohtani, H. Sakamoto, A. Ito, Y. Bai, Z. L. Wang, Y. Yamauchi and T. Fujita, *ACS Nano*, 2022, **16**, 20851–20864.
35 J. Nicks, S. A. Boer, N. G. White and J. A. Foster, *Chem. Sci.*, 2021, **12**, 3322–3327.
36 C. Guo, Y. Gao, S. Li, Y. Wang, X. Yang, C. Zhi, H. Zhang, Y. Zhu, S. Chen, S. Chou, S. Dou, Y. Xiao and X. Luo, *Adv. Funct. Mater.*, 2024, **34**, 2314851.
37 W. Qin, D. Si, Q. Yin, X. Gao, Q. Huang, Y. Feng, L. Xie, S. Zhang, X. Huang, T. Liu and R. Cao, *Angew. Chem., Int. Ed.*, 2022, **61**, e202202089.
38 Q. Yin, K. Pang, Y.-N. Feng, L. Han, A. Morsali, X.-Y. Li and T.-F. Liu, *Nat. Commun.*, 2024, **15**, 634.
39 S. Feng, Y. Shang, Z. Wang, Z. Kang, R. Wang, J. Jiang, L. Fan, W. Fan, Z. Liu, G. Kong, Y. Feng, S. Hu, H. Guo and D. Sun, *Angew. Chem., Int. Ed.*, 2020, **132**, 3868–3873.
40 J. Feng, T. Liu and R. Cao, *Angew. Chem., Int. Ed.*, 2020, **59**, 22392–22396.
41 A. A. Zhang, Y. L. Li, Z. Bin Fang, L. Xie, R. Cao, Y. Liu and T. F. Liu, *ACS Appl. Mater. Interfaces*, 2022, **14**, 21050–21058.
42 B. Han, H. Wang, C. Wang, H. Wu, W. Zhou, B. Chen and J. Jiang, *J. Am. Chem. Soc.*, 2019, **141**, 8737–8740.
43 B. Yu, T. Meng, X. Ding, X. Liu, H. Wang, B. Chen, T. Zheng, W. Li, Q. Zeng and J. Jiang, *Angew. Chem., Int. Ed.*, 2022, **61**, e202211482.
44 Z. Yang, Y. Zhang, W. Wu, Z. Zhou, H. Gao, J. Wang and Z. Jiang, *J. Membr. Sci.*, 2022, **664**, 121118.
45 H. Yang, C. Li, T. Liu, T. Fellowes, S. Y. Chong, L. Catalano, M. Bahri, W. Zhang, Y. Xu, L. Liu, W. Zhao, A. M. Gardner, R. Clowes, N. D. Browning, X. Li, A. J. Cowan and A. I. Cooper, *Nat. Nanotechnol.*, 2023, **18**, 307–315.
46 X. T. He, Y. H. Luo, D. L. Hong, F. H. Chen, Z. Y. Zheng, C. Wang, J. Y. Wang, C. Chen and B. W. Sun, *ACS Appl. Nano Mater.*, 2019, **2**, 2437–2445.
47 A. Kaushik, K. Marvaniya, Y. Kulkarni, D. Bhatt, J. Bhatt, M. Mane, E. Suresh, S. Tothadi, K. Patel and S. Kushwaha, *Chem*, 2022, **8**, 2749–2765.
48 W. Li, Y. Li, J. Caro and A. Huang, *J. Membr. Sci.*, 2022, **643**, 120021.
49 X. T. Jiang, Q. Yin, B. T. Liu, J. Y. Chen, R. Wang and T. F. Liu, *Nanoscale Adv.*, 2021, **3**, 3441–3446.
50 K. Han, C. Tan, S. Feng, Q. Zhang, X. Qiao, Z. Zhong, X. Wang, J. Meng and L. Mai, *Adv. Funct. Mater.*, 2025, **35**, 2407452.
51 C. A. Halliwell, K. Jolley, K. Yendall, M. R. J. Elsegood, G. N. Parkinson and A. Fernandez, *Angew. Chem., Int. Ed.*, 2024, **63**, e202404452.
52 R. Gao, R. Shen, C. Huang, K. Huang, G. Liang, P. Zhang and X. Li, *Angew. Chem., Int. Ed.*, 2025, **64**, e202414229.
53 H. Shi, D. Feng, H. Li, D. Yu and X. Chen, *J. Photochem. Photobiol., A*, 2023, **435**, 114292.
54 J. Li, H. Wang, D. Guan, X. Wang, C. Miao and J. Xu, *Adv. Mater.*, 2025, **37**, 2500721.
55 X. Zhang, W. Liu, F. Han, L. Jiang and Z. Li, *Appl. Surf. Sci.*, 2024, **644**, 158770.
56 Z. Li, B. Yu, Y. Wang, B. Yan, J. Liu, Y. Liu, R. Wang, P. Rao and Y. Liu, *ACS Appl. Mater. Interfaces*, 2025, **17**, 52981–52992.
57 B. T. Liu, X. H. Pan, D. Y. Zhang, R. Wang, J. Y. Chen, H. R. Fang and T. F. Liu, *Angew. Chem., Int. Ed.*, 2021, **60**, 25701–25707.
58 J. Xiao, A. R. M. Shaheer, C. Liu, T. Liu and R. Cao, *Aggregate*, 2024, **5**, e481.
59 Y. Wang, J. Yao, S. Wu, C. Zhi, L. Yin, Z. Song, J. Wang, L. Ling, Y. Ma, D. Zhang, J. Li, L. Li and B. Chen, *Chem*, 2025, **11**, 102457.
60 Z. Cheng, Y. Fang, Y. Yang, H. Zhang, Z. Fan, J. Zhang, S. Xiang, B. Chen and Z. Zhang, *Angew. Chem., Int. Ed.*, 2023, **62**, e202311480.
61 H. Naz, R. N. Ali, W. A. Qureshi, A. Ali, N. A. Albert and G. Zhu, *Sustain. Energy Fuels*, 2024, **8**, 3174–3181.
62 C. Wang, Y. Wang, K. O. Kirlikovali, K. Ma, Y. Zhou, P. Li and O. K. Farha, *Adv. Mater.*, 2022, **34**, 2202287.
63 J.-C. Liu, T. Li, P.-Y. Liao, Z.-Y. Ruan, Z.-H. Wang, J.-H. Jia and M.-L. Tong, *Sci. China: Chem.*, 2025, **68**, 4847–4855.
64 G. Chen, S. Huang, X. Ma, R. He and G. Ouyang, *Nat. Protoc.*, 2023, **18**, 2032–2050.
65 W. Huang, H. Yuan, H. Yang, L. Tong, R. Gao, X. Kou, J. Wang, X. Ma, S. Huang, F. Zhu, G. Chen and G. Ouyang, *JACS Au*, 2022, **2**, 2048–2058.
66 X. Zhao, Q. Yin, X. Mao, C. Cheng, L. Zhang, L. Wang, T.-F. Liu, Y. Li and Y. Li, *Nat. Commun.*, 2022, **13**, 2721.

67 H. Yang, J. Fu, W. Huang, T. Wu, S. Huang, G. Chen and G. Ouyang, *Small Struct.*, 2023, **4**, 2200346.
68 W. Li, J. Shi, Y. Chen, X. Liu, X. Meng, Z. Guo, S. Li, B. Zhang and Z. Jiang, *Chem. Eng. J.*, 2023, **468**, 143609.
69 J. Tang, J. Liu, Q. Zheng, W. Li, J. Sheng, L. Mao and M. Wang, *Angew. Chem., Int. Ed.*, 2021, **60**, 22315–22321.
70 Y. Cai, J. Gao, J. Li, P. Liu, Y. Zheng, W. Zhou, H. Wu, L. Li, R. Lin and B. Chen, *Angew. Chem., Int. Ed.*, 2023, **62**, e202308579.
71 G. Chen, S. Huang, Y. Shen, X. Kou, X. Ma, S. Huang, Q. Tong, K. Ma, W. Chen, P. Wang, J. Shen, F. Zhu and G. Ouyang, *Chem*, 2021, **7**, 2722–2742.
72 Z. Tang, X. Li, L. Tong, H. Yang, J. Wu, X. Zhang, T. Song, S. Huang, F. Zhu, G. Chen and G. Ouyang, *Angew. Chem., Int. Ed.*, 2021, **60**, 23608–23613.
73 J. Yang, Q. Jiang, Y. Chen, Q. Wen, X. Ge, Q. Zhu, W. Zhao, O. Adegbite, H. Yang, L. Luo, H. Qu, V. Del-Angel-Hernandez, R. Clowes, J. Gao, M. A. Little, A. I. Cooper and L. N. Liu, *ACS Catal.*, 2024, **14**, 18603–18614.
74 D. Lei, Y. Wang, Q. Zhang, S. Wang, L. Jiang and Z. Zhang, *Nat. Commun.*, 2025, **16**, 754.
75 K. Ma, P. Li, J. H. Xin, Y. Chen, Z. Chen, S. Goswami, X. Liu, S. Kato, H. Chen, X. Zhang, J. Bai, M. C. Wasson, R. R. Maldonado, R. Q. Snurr and O. K. Farha, *Cell Rep. Phys. Sci.*, 2020, **1**, 100024.
76 Y. J. Hou, S. Fang, X. Y. Zhang, J. Wang, Q. Ruan, Z. Xiang, Z. Wang and X. J. Zhu, *ACS Appl. Mater. Interfaces*, 2022, **14**, 49875–49885.
77 H. R. Li, S. Wu, X. Jing, Z. Di, K. Liu, L. Wang, C. P. Li, Z. Liu and M. Du, *Sci. China: Chem.*, 2024, **67**, 2958–2967.
78 R. Li, X. Chen, Z. Bian, R. Yu, Y. Chen, J. Zhang, J. Wang and X. Feng, *J. Alloys Compd.*, 2025, **1020**, 179345.
79 L. Giri, B. Mohanty, R. Thapa, B. K. Jena and V. R. Pedireddi, *ACS Omega*, 2022, **7**, 22440–22446.
80 Q. Zhou, Y. Guo and Y. Zhu, *Nat. Catal.*, 2023, **6**, 574–584.
81 B. Yu, L. Li, S. Liu, H. Wang, H. Liu, C. Lin, C. Liu, H. Wu, W. Zhou, X. Li, T. Wang, B. Chen and J. Jiang, *Angew. Chem., Int. Ed.*, 2021, **60**, 8983–8989.
82 L. Yang, J. Yuan, G. Wang, Q. Cao, C. Zhang, M. Li, J. Shao, Y. Xu, H. Li and J. Lu, *Adv. Funct. Mater.*, 2023, **33**, 2300954.
83 G. Chen, L. Tong, S. Huang, S. Huang, F. Zhu and G. Ouyang, *Nat. Commun.*, 2022, **13**, 4816.
84 J. Tang, J. Liu, Q. Zheng, R. Yao and M. Wang, *Angew. Chem., Int. Ed.*, 2023, **62**, e202312784.
85 C. Huang, C. Zhao, Q. Deng, H. Zhang, D. Yu, J. Ren and X. Qu, *Nat. Catal.*, 2023, **6**, 729–739.
86 P. Luo, C. Zheng, J. He, X. Tu, W. Sun, H. Pan, Y. Zhou, X. Rui, B. Zhang and K. Huang, *Adv. Funct. Mater.*, 2022, **32**, 2107277.
87 B. Yu, J. Xing, P. Zhang, R. Gao, S. Lin, K. Jiang and L. Zhang, *Inorg. Chem.*, 2025, **64**, 1258–1262.
88 Y. Liang, R. An, P. Du, P. Lei and H. Zhang, *Nano Today*, 2023, **48**, 101751.
89 Y. Nie, D. Li, Y. Peng, S. Wang, S. Hu, M. Liu, J. Ding and W. Zhou, *Int. J. Pharm.*, 2020, **585**, 119513.
90 W. Wang, Y. Shi, W. Chai, K. W. K. Tang, I. Pyatnitskiy, Y. Xie, X. Liu, W. He, J. Jeong, J. C. Hsieh, A. R. Lozano, B. Artman, X. Shi, N. Hoefer, B. Shrestha, N. B. Stern, W. Zhou, D. W. McComb, T. Porter, G. Henkelman, B. Chen and H. Wang, *Nature*, 2025, **638**, 401–410.